A COMPARATIVE STUDY ON THE CONTROL OF ACTIVE MAGNETIC BEARINGS

A dissertation presented to

The School of Electrical, Electronic and Computer Engineering

North-West University

In partial fulfilment of the requirements for the degree

Magister Ingeneriae

in Electrical and Electronic Engineering

by

J.D.Z. Stott

Supervisor: Prof. G. van Schoor
Assistant Supervisor: Mr. E.O. Ranft

December 2005

Potchefstroom Campus

Summary

The aim of this project is to perform a comparative study on different control techniques applied to active magnetic bearings (AMBs). The project will involve the evaluation of two suitable nonlinear modern control techniques on an existing model to illustrate their superior performance over conventional linear control techniques. The techniques under investigation are classical PD control, fuzzy logic control and sliding mode control.

As a first step the experimental model was characterised and found to be inadequate for a meaningful comparative control study. The physical model was improved in terms of sensor linearisation, power amplifier configuration and magnetic circuit layout. A comprehensive matched simulation model of the experimental model is then developed to serve as the design platform for the mentioned controllers.

The comparative study commences with the optimisation of a classical PD controller for the experimental model. This controller is used as benchmark for performance comparison. An equivalent linear fuzzy logic controller is then derived from the PD controller. Finally a control law is derived for a sliding mode controller.

The performances of the different controllers are evaluated for step inputs of 1000, 200 and 1500 μm respectively. The simulated PD and fuzzy logic responses showed remarkable correlation as well as the experimental results. The sliding mode controller is simulated and intuitively optimised. The simulated and practical responses of the sliding mode controller also showed good correlation. Some differences in the response are attributed to implementation discrepancies.

The controllers are compared in terms of the equivalent stiffness and damping of the different systems. The ITAE performance index is used as an additional comparative criterion and identified the sliding mode controller as superior to the linear controllers.

This project emphasises the importance of accurate modelling. Future work will involve delinearisation of the fuzzy logic controller and a specialised study on sliding mode control.

Opsomming

Die doelwit van hierdie projek is om 'n vergelykende studie te doen op verskillende beheertegnieke wat van toepassing is op aktiewe magnetiese laers (AMLs). Die projek behels die evaluering van twee toepaslike nie-liniêre moderne beheertegnieke op `n bestaande model om hul oortreffende prestasie bo konvensionele liniêre beheertegnieke te illustreer. Die beheertegnieke wat ondersoek word is klassieke PD beheer, wasige logiese beheer en glymodus beheer.

As 'n eerste stap is die eksperimentele model gekarakteriseer en daar is gevind dat dit onvoldoende was vir 'n sinvolle vergelykende beheerstudie. Die praktiese model is verbeter in terme van sensorlinearisering, kragversterkerkonfigurasie en magnetiese baan uitleg. 'n Omvattende, versoende simulasiemodel is van die eksperimentele model ontwikkel om as ontwerpplatform vir die genoemde beheerders te dien.

Die vergelykende studie neem 'n aanvang met die optimering van 'n klassieke PD beheerder vir die eksperimentele model. Hierdie beheerder word as die vergelykende maatstaf gebruik vir die prestasievergelyking. 'n Ekwivalente liniêre wasige logiese beheerder word dan van die PD beheerder afgelei. Uiteindelik word 'n beheerwet vir die glymodus beheerder afgelei.

Die prestasie van die verskillende beheerders word geëvalueer vir trapinsette van 1000, 200 en 1500 μm onderskeidelik. Die PD en wasige logiese response het merkwaardige ooreenstemming getoon vir beide die gesimuleerde en eksperimentele resultate. Die glymodus beheerder is gesimuleer en intuïtief geoptimeer. Die gesimuleerde en praktiese response van die glymodus beheerder het ook goeie korrelasie getoon. Sommige verskille in die response word toegeskryf aan implementerings diskrepansies.

Die beheerders word vergelyk in terme van hul ekwivalente styfhede en demping vir die verskillende stelsels. Die ITAE prestasieindeks word gebruik as 'n bykomende vergelykingskriterium en het die glymodus beheerder as die oortreffende beheerder geïdentifiseer.

Die projek beklemtoon die belangrikheid van akkurate modellering. Verdere werk sal die delinearisering van die wasige logiese beheerder en 'n gespesialiseerde studie op glymodusbeheer insluit.

Acknowledgements

I would like to thank M-Tech Industrial and THRIP for funding this research.

I would also like to acknowledge the following people, in no particular order, for their contributions during the course of this project.

- Professor George van Schoor, my supervisor, for his inspiration, guidance, advice and management.

- Eugèn Ranft, for his technical support, advice, friendship and motivation.

- Andrè Nieman, for his practical support, help and friendship.

- My family for their love, motivation and support.

- My friends, Charl, Deon, Hannes and Rudi, for their motivation and help.

"Make sure your dreams are big enough for God to fit in"

Table of contents

List of figures

List of tables

List of abbreviations

AMB	Active Magnetic Bearing
dc	Direct current
MOSFET	Metal-oxide semiconductor field-effect transistor
MRAC	Model reference adaptive controller
PA	Power Amplifier
PBMR	Pebble Bed Modular Reactor
PC	Personal Computer
R&D	Research and developement
rms	Root mean square
rpm	Revolutions per minute
STC	Self-tuning controller
VSCS	Variable Structure Control System

List of symbols

A_g	Air gap area

b_{eq}	Equivalent damping
C	Capacitance
F, F_m	Electromagnetic force
g, g_0	Air gap length
i	Instantaneous current
i, i_0, i_m	Control, bias and electromagnet currents respectively
k_d	Differential gain of the PD controller
k_{eq}	Equivalent position stiffness
k_i	Force-current factor
k_m	Electromagnet constants
k_p	Proportional gain of the PD controller
k_s	Force-displacement factor
ℓ	Magnetic path length
L_c	Coil inductance
m	Suspended body mass / current slope
N	Number of coil turns
P	Electrical power
$P.O.$	Percentage overshoot
R	Electrical resistance
R_{coil}	Coil resistance
s	Complex frequency
T_s	Settling time
V	rms / dc value of voltage
v	Instantaneous voltage
x, x_0, x_s	Rotor position
ω	Rotational speed
ω_n	Natural frequency
ζ	Damping factor
Φ	Magnetic flux

Chapter 1

Introduction

Chapter 1 supplies preliminary information on the pebble bed modular reactor control and active magnetic bearings in general. The problem statement is given, followed by the issues to be addressed and the methodology used. A concise overview of the document is also presented.

1.1 Background

The School of Electrical, Electronic and Computer Engineering at the North-West University is in the process of developing an Active Magnetic Bearing (AMB) research laboratory. The aim is to establish a knowledge base on AMBs in support of industries that make use of this environmentally friendly technology. AMB technology is seen as one of the technology drivers for the Pebble Bed Modular Reactor (PBMR) currently in development in South Africa and is predicted to become largely conventional in this application.

1.1.1 The Pebble Bed Modular Reactor

The Pebble Bed Modular Reactor (PBMR) is a small, clean, cost effective and inherently safe nuclear power plant. It uses coated uranium particles encased in graphite to form a fuel sphere (60 mm in diameter). The PBMR design makes use of helium as the coolant and energy transfer medium to a closed cycle gas turbine and generator.

The PBMR represents the new generation of advanced nuclear reactors characterized by their inherent safety properties. This feature, which renders the need for safety grade backup systems and off-site emergency plans obsolete, is fundamental to the cost reduction achieved over other nuclear reactor designs.

Based on the belief that new generation nuclear reactors should be small, the PBMR is being designed in a modular form. This design not only allows the erection of small power plants to serve local needs, but also makes provision for expansion as demand grows. Dry cooling, although more expensive, is an option to provide even more freedom of location [1].

The primary objective of the PBMR is to achieve a plant that has no physical process that could cause a radiation hazard beyond the reactor boundary. Producing approximately 110 MW of electrical power the PBMR module is the smallest standalone component of the PBMR power generation system. The module can produce power in a standalone mode, or as part of a power plant that consists of up to ten units [1].

To prevent nuclear contamination to the environment helium gas is used as coolant because it is chemically and radiologically inert. If for some reason the helium would escape from the system into the atmosphere it will not hold a contamination risk for the environment. The only other possible source of nuclear contamination in the gas cycle would be oil from the oil film bearings of the compressors, power turbine and generator. For this reason bearings that do not use any kind of lubrication are used [2].

1.1.2 Active Magnetic Bearings

According to Kasarda [3], patents associated with passive, active and hybrid magnetic bearings go back more than 150 years. The earliest patents focused on passive systems involving permanent magnets, which proved problematic in terms of rotor positioning and or stability. As early as 1842, theory existed that a three-axis passive suspension system was unstable. It was not until active control systems came into being, that full magnetic suspension of a system could practically be obtained for many applications.

Jesse Beam, a physics professor at the University of Virginia, explored methods of active magnetic levitation using electromagnets for high speed rotors. It is interesting to note that in the context of his research, Beam worked on methods for spinning small steel balls at high speeds and received a patent for a device with a rotational speed of four million revolutions per second.

To support a spinning rotor, five axes of support are necessary: two radial bearings, each with two suspension axes, and an axial axis realising the fifth. Although early researchers laid the groundwork for useful magnetic levitation devices, it was not until the introduction of high-speed electronics that magnetic bearings became an economically and technically viable option for operation as a support bearing system for high-speed rotating equipment.

The success of modern magnetic bearings can be attributed to one of the first commercial magnetic bearings companies, S2M. This company was created by a joint venture between the French Societe Europeene de Propulsion (SEP) and the Swedish company SKF in 1976. The first commercial marketing of AMBs by S2M focussed on the turbomachinery sector.

- **Advantages**

Advantages of the AMB include no wear and no lubrication requirements. AMB technology is an environmentally friendly technology that results in the reduction of equipment maintenance and waste associated with the replacement of used lubricants and bearings. The no-lubrication aspect of this technology also makes it ideal for operation in vacuum environments, space-based applications and situations where minimal maintenance is critical.

Another major advantage of AMBs is that they are capable of operating under much higher speeds than conventional rolling element bearings with relatively low power losses. The upper limits on rotating machinery supported in AMBs are most likely due to limits associated with shaft material or rotor assembly during high-speed operation.

- **Disadvantages**

One of the major barriers facing designers and users of AMBs is addressing the problem of what happens when the power to the AMB is cut. Power outages result in rapidly delevitated rotors. Under this condition, AMBs must be supported by passive backup bearings.

The lower load capacity of AMBs per volume necessitates a larger installation area.

Economics also play a major role in dictating and limiting the use of AMBs. Although the price of AMBs continues to decrease in general, they still tend to be quite costly from an initial layout standpoint. A long-term payback analysis including reduction in maintenance cost is necessary for economic justification in some cases.

1.1.3 Control

AMB systems are inherently open-loop unstable. According to Earnshaw's theorem no stationary object made of magnets in a fixed configuration can be held in stable equilibrium by any combination of static magnetic or gravitational forces. Earnshaw's theorem can be viewed as

a consequence of the Maxwell equations, which do not allow the magnitude of a field in a free space to possess a maximum, as required for stable equilibrium. By using some kind of active control the system can be stabilised.

A control system is an interconnection of components forming a system configuration that will provide a desired system response [4]. Linear system theory provides the basis for the analysis of a system. The theory is based on a cause and effect relationship between the components of the system and therefore the process to be controlled can be presented by a block as shown in Figure 1.1.

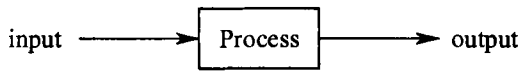

Figure 1.1: Process representation

The input-output relationship depicts the cause-and-effect relationship of the process. This represents the input being processed to result in an output variable which normally contains amplification. An open-loop system uses a controller to produce the desired response of the system without feedback, illustrated in Figure 1.2.

Figure 1.2: Open-loop control system

A closed loop system uses a measure of the output of the system to compare the actual output to the desired output response of the system. The measure of the output is called the feedback signal of the system. A basic closed-loop feedback control system is shown in Figure 1.3.

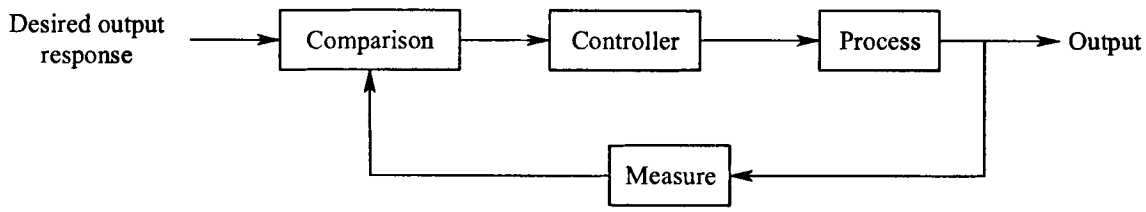

Figure 1.3: Closed-loop feedback control system

A feedback control system normally uses a function of a prescribed relationship between in desired state of the output and the output to control the process. Usually the difference between

the desired state and the output of the process is amplified and used to control the process to continually reduce the difference. The feedback concept is the foundation for control analysis and design [4].

Feedback controllers in turn can be divided into linear and nonlinear controllers. Knowing that AMB systems are highly nonlinear the suitability of nonlinear controllers on AMBs will be investigated in this study and compared to linear controllers.

The principle that is most often used to obtain magnetic suspension is that of the active electromagnetic bearing. Figure 1.4 explains the components and the function of a simple AMB. A sensor measures the displacement of the rotor from the reference position. A controller then derives the appropriate control signal which is converted into a control current by the power amplifier (PA). The control current then generates the magnetic forces required within the electromagnetic actuator to stably suspend the rotor at the reference position [5].

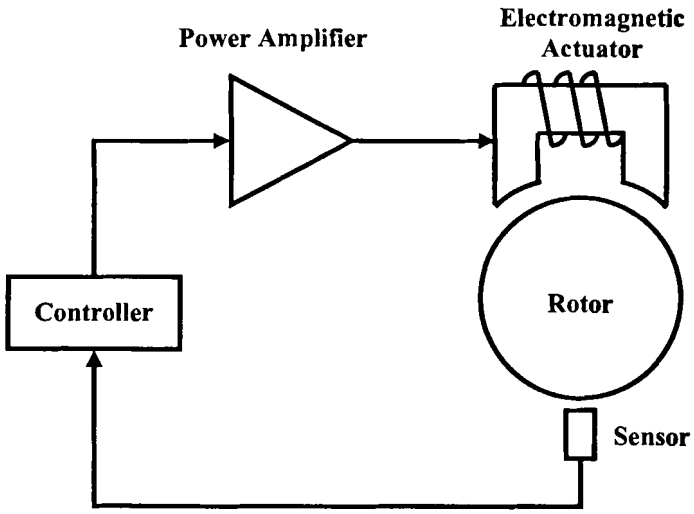

Figure 1.4: AMB functional diagram [5]

1.2 Problem statement

The purpose of this study is to perform a comparative study on different control techniques applied to AMBs. The project will involve the evaluation of two suitable nonlinear modern control techniques on developed models to illustrate their superior performance over conventional linear control techniques. The nonlinear control techniques to be investigated are a

fuzzy logic controller and a sliding mode controller. The linear controller which serves as the benchmark for the comparative study is a PD controller.

1.3 Issues to be addressed and methodology

1.3.1 Evaluation platform

An experimental model has to be identified and modified to render it suitable for the comparison between the different controllers. A comprehensive simulation model must be developed in MATLAB® and matched to the experimental model to form the evaluation platform.

1.3.2 Controller identification

A thorough literature study on the control of AMBs has to be done. From the study two of the most promising nonlinear control techniques must be identified to be evaluated on the evaluation platform.

1.3.3 Controller implementation

After the two most applicable controllers are identified they will firstly be implemented on the developed simulation platform to determine whether they are suitable for practical implementation. After the suitability of the controllers are determined, the controllers must be implemented on the experimental platform. A linear PD controller will also be implemented on both platforms to serve as a comparative benchmark. dSPACE® real-time technology will be used to implement the controllers on the experimental platform.

1.3.4 Controller comparison

When the controllers have been successfully implemented on both platforms, they will be compared by using a linear PD controller as the benchmark. Different performance indices will be identified and the most suitable ones will be used for the comparative evaluation. The equivalent stiffness and equivalent damping of the AMB system will be used to compare the identified controllers. The ITAE performance indices of the different controllers for step responces will also be compared.

1.4 Synopsis of dissertation

Chapter 2 contains a literature study describing the basic principles of some advanced control techniques which are applicable to AMBs.

In chapter 3 the evaluation platform for the comparative study is discussed. A detailed simulation platform of the experimental platform is created and implemented using MATLAB®. The basic procedure followed for control system design will also be discussed in chapter 3.

Chapter 4 describes the implementation of a linear PD controller and an equivalent linear fuzzy logic controller on the evaluation platform. A linear model of the AMB as well as an equivalent linear fuzzy logic controller is derived in the chapter.

Nonlinear control is covered in chapter 5. The background to sliding mode control is discussed and a sliding mode control law is derived for an AMB system operated in the differential driving mode. This control law is also implemented on both the simulation and experimental platforms.

Finally the different controllers are compared in chapter 6. Concluding remarks as well as recommendations for future work are given.

Chapter 2

Modern control techniques

Although AMBs are inherently highly nonlinear most of the control design used in practice is based on linear control theory. Recently a tremendous amount of research has been done on the applications of nonlinear control theory and therefore more effective control techniques which account for system nonlinearities can be applied to the AMB control problem.

In this chapter the basic principles of some advanced control techniques which are applicable to AMBs will be briefly studied to determine which two nonlinear control techniques will be compared to the classical linear PD control technique.

2.1 Introduction to nonlinear control

The science of automatic control deals with the identification, analysis and design of dynamic systems. Even though the design of an automatic control system will include the aspect of control and a satisfactory system may not be achieved without feedback, it is also necessary that a considerable amount of attention has to go into the analysis of the system by using the theory of dynamic systems.

The majority of the theory available is concerned with linear time invariant systems. Unfortunately no physical system belongs to the class of linear time invariant systems. This obviously does not mean that the theory of nonlinear time invariant systems is of no use, but that it has limitations and it may be essential to have theories that consider nonlinearities and time dependence.

A nonlinear system may be defined as one to which the principle of superposition does not apply. This means that it is not possible to determine the response of the system for a particular input if the response to a different input is known.

Many researchers and designers have shown great interest in the development and application of nonlinear control methodologies. Some of the reasons are:

- **Improvement of existing control systems**

Linear control methods rely on the assumption that the operating range of the system is small for the linear model to be valid. If the applicable operating range is large, a linear controller may perform poorly or the system might be unstable because the controller may not be able to compensate for the nonlinearities of the system. Nonlinear controllers can cater for these nonlinearities over a large operating range.

- **Analysis of hard nonlinearities**

Another assumption of linear control is that the system model is indeed linearizable. In many cases of control systems, linear approximation is not possible due to the nature of the systems nonlinearities. These nonlinearities include saturation, dead zones, backlash and hysteresis and are often found in control systems. Their effects cannot be derived from linear methods, and nonlinear analysis techniques have to be employed to predict the systems performance in the presence of these inherent nonlinearities. These nonlinearities frequently cause undesirable behaviour such as instability or limit cycles. Therefore they have to be predicted and effectively compensated for.

- **Model uncertainties**

In designing linear controllers it is usually necessary to assume that the parameters of the system model are reasonably well known. However, in many systems there are model parameter uncertainties which may be due to a slow time variation or an abrupt change. A linear controller based on inaccurate model parameters may exhibit performance degradation or may even become unstable. Nonlinearities can intentionally be introduced to the controller part of the system so that model uncertainty can be tolerated.

- **Design simplicity**

Good nonlinear control designs may be simpler and more intuitive than their linear counterparts. This is due to the fact that nonlinear controller designs are often deeply rooted in the physics of the plant for example a pendulum's stability can not be determined by the eigenvalues of its linearised system matrix but comes from the fact that the total mechanical energy of the system is dissipated by various friction forces. The pendulum therefore comes to rest at a position of minimal energy [5].

2.2 Nonlinear control techniques

2.2.1 Feedback linearisation

Feedback linearisation is a versatile control technique for nonlinear systems which converts nonlinear system dynamics into a (fully or partly) linear system so that linear control techniques can be used. This is done by using a nonlinear coordinate transformation and feedback control which differs completely from conventional linearisation in that feedback linearisation is done by exact state transformations and feedback opposed to linear approximations of the dynamics. The effect is a conversion or input signal that contains a linear and a nonlinear component. These techniques can be viewed as ways of converting original system models into equivalent but simpler system models.

Feedback linearisation has successfully been implemented on practical control problems such as the control of helicopters, high performance aircraft, industrial robots and biomedical devices [5].

Feedback linearisation has a number of shortcomings and limitations. It may result not only in wasteful controls, but also in nonrobust systems. This may happen because feedback linearising control laws often destroy inherently stabilizing nonlinearities and replace them with destabilizing terms and therefore cannot be used for all nonlinear systems. Other drawbacks are that the full state of the system has to be measured and robustness cannot be guaranteed in the presence of parameter uncertainties or unmodelled dynamics [7].

2.2.2 Adaptive control

Adaptive controllers are used in systems with slow varying or constant uncertain parameters, for example aircrafts where the dynamics of the aircraft change with speed, altitude and pitch angle. Another example is a ship's roll damper which takes the frequency of the waves into account.

The basic idea behind adaptive control is to estimate uncertain plant parameters on-line, based on measured system signals and then use the estimated parameters to compute the control input. An adaptive controller is therefore a controller with adjustable parameters and a mechanism for adjusting the parameters.

There are two main approaches for designing adaptive controllers. The one is the model reference adaptive controller (MRAC) and the other is the self-tuning controller (STC).

- **Model reference adaptive control**

The model-reference adaptive controller basically consists of four components namely a plant with some unknown parameters, a reference model to specify the desired output of the system, a feedback control law with adjustable parameters and a mechanism to update the adjustable parameters. Figure 2.1 shows the functional diagram of a MRAC system.

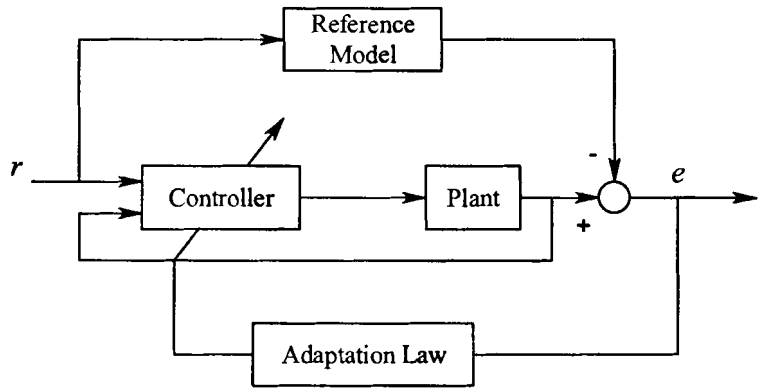

Figure 2.1: Block diagram of a model reference adaptive control system

The plant is assumed to have a known structure, although the parameters are unknown. For example in a linear plant the order of the system may be known but the position of the poles and zeros of the plant may be unknown and in a nonlinear plant such as an AMB system the structure of the dynamics may be known but the system parameters might not.

The reference model is used to specify the ideal response of the adaptive system to external commands. It provides the adaptive mechanism a response to imitate by adjusting the controller parameters. Part of adaptive control system design is to choose a reference model that should reflect the performance specification in the control tasks and the ideal behaviour should be achievable for the adaptive control system.

The controller is normally parameterized by a number of adjustable parameters which implies that a family of controllers can be defined by assigning various values to the adjustable parameters. The controller should have perfect tracking capacity to allow the possibility of convergence. This means that if the plant parameters are exactly known, the corresponding

parameters of the controller will result in a plant output that is identical to the output of the reference model and if the plant parameters are not known the adaptation mechanism will adjust the controller parameters so that perfect tracking is achieved asymptotically.

The adaptation mechanism is used to adjust the parameters of the controller. In MRAC systems the adaptation law searches for parameters such that the response of the plant resembles that of the reference model. The main difference between conventional and adaptive control lies with the adaptation mechanism.

- **Self-tuning controllers**

During conventional controller design the parameters of the controller are determined directly from the parameters of the plant or process. If the parameters of the plant are not known estimates of the plant are updated and the controller parameters are obtained from the solution of an estimator algorithm by using the estimated plant parameters. Figure 2.2 shows the block diagram of a self tuning control system

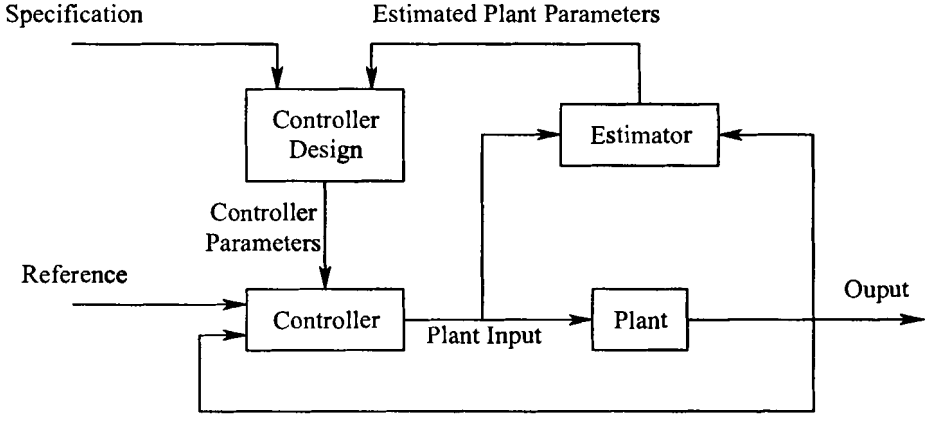

Figure 2.2: Block diagram self-tuning controller system

This controller basically consists of two control loops. The inner loop consists of the plant and a normal feedback controller. The outer loop adjusts the parameters of the controller and consists of a recursive parameter estimator and a design calculation. The system can be seen as an automation of plant modelling and design where the plant model and the control design are updated with every sample period [8].

2.2.3 Sliding mode control

Many models in control systems are imprecise. Model imprecision can be attributed to unknown parameters in the plant or to the intentional simplification of the system's dynamics.

Modelling inaccuracies can be categorized as follows:

- Parametric uncertainties
- Unmodelled dynamics

Parametric uncertainties incorporate inaccuracies due to parameters which are included in the model, but were chosen incorrectly, while unmodelled dynamics correspond to inaccuracies in the system order.

Modelling inaccuracies may cause significant performance degradation or even instability. Two major and complimentary approaches to negotiate these problems are robust and adaptive control.

Sliding mode control is a simple approach to robust control and is based on the fact that it is easier to control a 1^{st}-order system than it is to control an n^{th}-order system. In this technique a notational simplification is introduced to replace n^{th}-order problems with equivalent 1^{st}-order problems. Perfect performance in the presence of parameter inaccuracies can be achieved using sliding mode control, but it is at the expense of very high control activity.

The advantages of sliding mode control is that it is a systematic approach to the problem of maintaining stability and consistent performance in the presence of modelling inaccuracies and by allowing trade-offs between modelling and performance to be quantified, the design process becomes easier to interpret [5].

2.2.4 Fuzzy logic control

Fuzzy control, unlike learning control and expert control, is built on mathematical foundations with fuzzy set theory. It represents knowledge or experience in a mathematical format such that process and system dynamic characteristics can be described by fuzzy sets and fuzzy relational

functions. Control decisions can be generated based on the fuzzy sets and functions with rules. Figure 2.3 illustrates the basic operation of a fuzzy system.

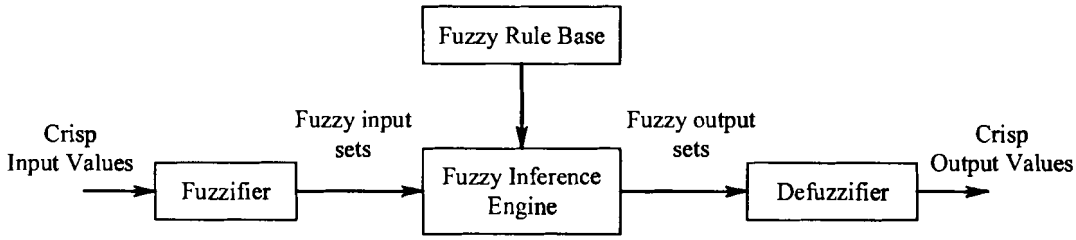

Figure 2.3: Block diagram of a fuzzy controller system

Although fuzzy control has great potential for solving complex control problems, its design procedure is complicated and requires a great deal of specialty. In addition, fuzzy mathematical operations do not belong to the field of classic mathematics since many basic mathematical operations do not exist. For instance, the inverse addition is not available in fuzzy mathematics. Then, it is very difficult to solve a fuzzy equation, yet solving a differential equation is one of the basic practices in traditional control theory and applications. Therefore, lack of good mathematical tools is a fundamental problem for fuzzy control to overcome.

2.2.5 Optimal control

The aim of optimal control is to determine the control signals that will cause a process to satisfy the physical specifications and at the same time minimize (or maximize) some performance criteria. Optimal control deals with the problem of finding a control law for a given system such that a certain optimality criterion is achieved [9].

2.3 Conclusion

In this chapter the basic principles of some nonlinear modern control techniques which are applicable to AMBs were discussed. From the study it became apparent that fuzzy logic and sliding mode controllers have previously been implemented on AMBs with reasonable success and were therefore identified as the two most appropriate nonlinear control techniques for the comparative study.

Chapter 3

Evaluation platform

For the purpose of this study system evaluation is performed via an experimental platform and a simulation platform. The experimental platform is a practical model on which the different controllers are compared while the simulation platform is a MATLAB® simulation on which the controllers were also compared before they are implemented practically. This chapter discusses the components of the different platforms. The system on which the study is performed is adopted from a previous study by Gouws [10].

3.1 Introduction

The implementation of a control system involves a number of systematic steps which can be represented by the flow diagram in Figure 3.1 [4].

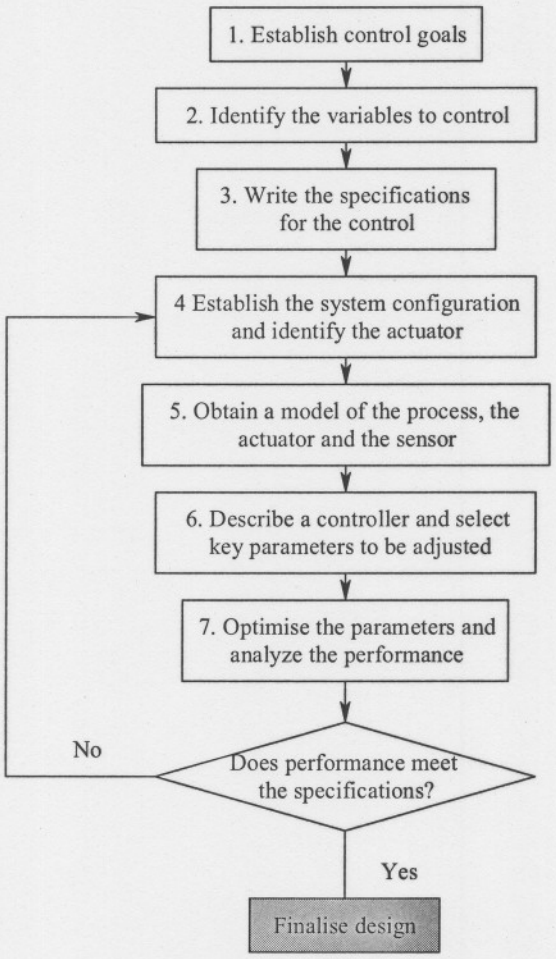

Figure 3.1: Design process

The steps in Figure 3.1 may not necessarily be performed in the specific order and the trial and error loop in the latter part of the process may involve repeated jumps between steps. The modelling stage of the process where mathematical relationships between various system variables are formulated is extremely important. The results and success of the entire system depend on this step because the model equations obtained here are used to design the controller. It is of no use doing intensive simulations and controller optimisation to a poorly modelled system. The models of the various elements of the system can be obtained from the basic physical laws governing their behaviour or by experimental measurement also known as identification.

During the design process of the controller steps 1 to 4 were not executed in the conventional manner as illustrated in Figure 3.1. The system on which the study was performed existed and the luxury of performing these steps was not possible. The following subparagraphs explain the process followed and documents the final status of the system.

3.1.1 Control goals

The goal of the design is to stably and robustly suspend a 2 kg steel disc at a distance of 3 mm.

3.1.2 Control variables identification

The control variable is the position of the disc.

3.1.3 Controller specifications

Distinct specifications for the behaviour of the system could not be obtained from the system design documentation by Gouws [10]. This however was not a major problem due to the fact that the intention is to optimise the response of the system for comparative purposes.

3.1.4 System configuration and actuator identification

Figure 3.2 shows the functional block diagram of the axial magnetic bearing.

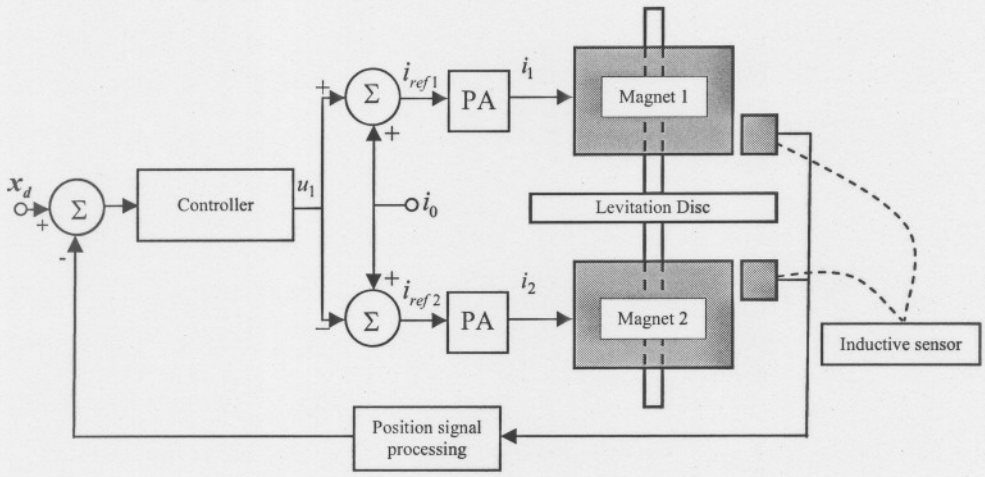

Figure 3.2: Axial AMB functional block diagram

A steel disk with a mass of 2 kg is suspended by two electromagnets, one above the disk and one below. The bottom magnet is included to enhance the bearing stiffness. An inductive sensor senses the position of the disc and generates a position sensitive signal. This signal is converted into a position signal by a position signal processing unit after which it is compared to a position reference to obtain an error signal. The error signal is compensated by the control algorithms to produce appropriate current reference signals for the power amplifiers (PAs). The PAs supply the electromagnets with the required current to suspend the disc at the required position.

3.1.5 Obtain model of process, actuator and sensor

During the characterisation of the system, fundamental problems were identified. Before the different controllers could be effectively implemented, alterations had to be made to the hardware of the system. A comprehensive model of the system could then be constructed using MATLAB®. This section of the design procedure is extensively covered in the remainder of the chapter.

3.1.6 Describe a controller and select key parameters to be adjusted

In chapter 2 the controllers identified to be implemented for the comparative study were a fuzzy logic controller and a sliding mode controller. These controllers will be implemented for the execution of this step along with a conventional PD controller. The PD controller will be implemented as a benchmark to compare the nonlinear controllers to. Chapters 4 and 5 deal with this step.

3.1.7 Optimise the parameters and analyse the performance

The optimisation of the system responses for the different controllers is dealt with in chapters 4 and 5. The method to be followed will be to intuitively optimise the system response when operating with the PD controller by adjusting the proportional and the derivative gains of the controller. An equivalent linear fuzzy logic controller will be designed and implemented to generate an equivalent response. Finally the sliding mode controller will be implemented and its controller variables intuitively adjusted for the best performance.

3.2 Experimental platform

The experimental platform is an existing axial AMB designed by Gouws [10]. During the modelling process of the design, it was discovered that the existing system would not be suitable for the specific study and the decision was taken to redesign the system. The problems identified on the system were the following:

(a) Magnetic circuit

A fundamental flaw was identified in the magnetic circuit. The guide bar connected to the levitation disc shown in Figure 3.3 was manufactured from ferromagnetic material. This caused the magnetic flux to leak past the inner air gap causing a significant reduction in magnetic force. The problem was addressed by replacing the bar with non-magnetic material.

(b) Power amplifiers

The PAs previously used on the system were voltage controlled PAs. The use of these amplifiers increases the complexity of the plant description and the controllers, rendering them unsuitable for the application. The PAs were substituted with current controlled amplifiers.

(c) Sensor

During the characterisation of the sensor it was found that the sensor was nonlinear. This problem was addressed by applying linearisation techniques. The sensor was also found to be very susceptible to noise. To address this problem, all the signal transmission cables were shielded which solved the problem to some extent.

Figure 3.3 depicts a schematic diagram of the experimental system under investigation.

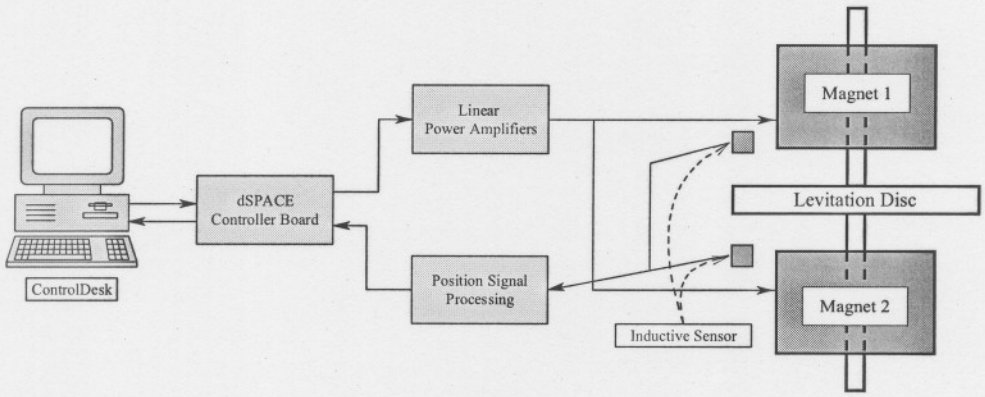

Figure 3.3: Basic experimental system diagram

The control algorithms that compensate the error signals are created in Simulink® and downloaded to a dSPACE DS1104 R&D Controller Board. The controller board then controls the system independently. ControlDesk software is installed on the host PC to change control parameters in real-time and to access system variables for development.

The system specifications are summarised in Table 3.1.

Table 3.1: Experimental model specifications

Parameter	Specification
Rotor base	140 mm
Rotor shaft diameter	10 mm
Length of base	15 mm
Length of shaft	260 mm
Rotor mass	2 kg
Operating position	3 mm
Maximum attraction distance	6 mm

3.2.1 Electromagnet

The actuator of the system is the combination of the two electromagnets mentioned in the previous paragraph and the power amplifiers. The diagram of one of the electromagnets is given in Figure 3.4 and the specifications in Table 3.2.

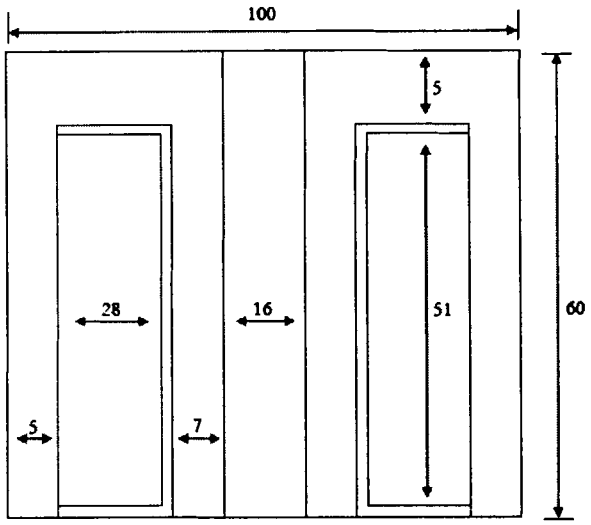

Figure 3.4: Electromagnet dimensions

Table 3.2: Actuator specifications

Specification	**Rating**
Inductance	400 mH
Number of turns	1250

3.2.2 Sensor

The sensor used in the study is an inductive sensor. This type of sensor operates with two inductive coils working as a pair, one on either side of the disc. If the position of the disc is varied, the impedances of the two coils vary accordingly. This variation is then used to determine the sensor output voltage which is representive of the position of the disc. A block diagram of the sensor is given in Figure 3.5.

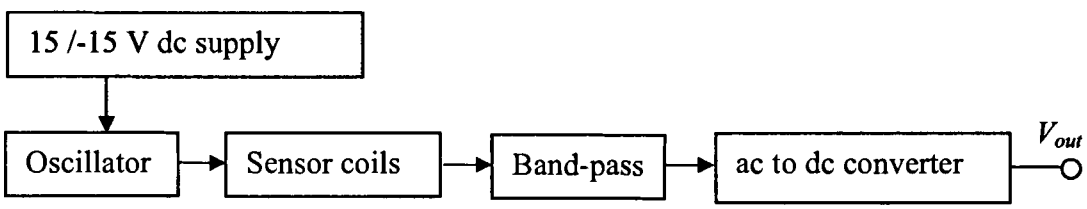

Figure 3.5: Inductive sensor operational block diagram

For a linear position response the sensor coils have to be placed as close as possible to the disc. The system specifications specify a relatively large rotor travel and therefore the distance

between the two coils are inherently large, impairing the linearity of the sensor. To be able to stably suspend the steel disk it is important that the position of the disk be accurately sensed and converted to a linearly corresponding voltage signal for it to be compared to the reference signal. The error can only then be effectively compensated by the implemented controller.

- **Sensor characterization**

The characterisation of the sensor is shown in Figure 3.6 and is clearly non-linear. The method originally used to linearise the sensor was to fit a fourth order polynomial to the measured data of the sensor. This polynomial is then used as a converter to convert the output voltage of the sensor into a linear position signal.

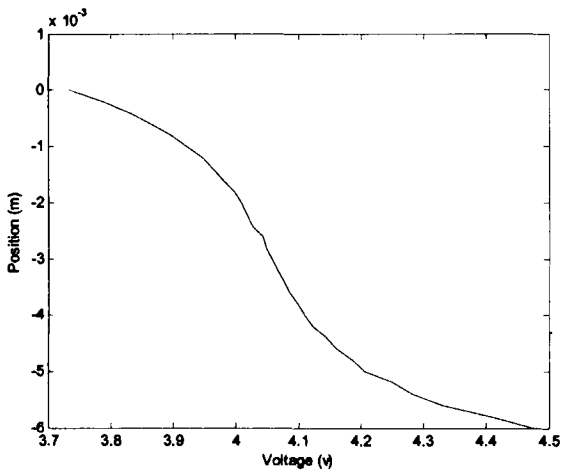

Figure 3.6: Characterisation of position sensor

The polynomial was fitted to the measured data with MATLAB® and is given by (1).

$$x = -8.143 \times 10^{-2} \cdot v^4 + 1.385 \cdot v^3 - 8.813 \cdot v^2 + 2.483 \times 10^{-1} \cdot v - 2.614 \times 10^{1} \quad (1)$$

where x is the position of the disk and v is the sensor voltage.

Figure 3.7(a) shows the comparison between measured sensor data and the fitted polynomial and reveals inaccuracy. An incorrect position of the disc will therefore be supplied to the controller which in turn causes incorrect compensation. The result of this scenario leads to an inaccurate and unstable system. To evaluate the effectiveness of the voltage to position converter, the actual position of the disk is plotted against the converter output in Figure 3.7(b). The figure shows that the sensor was not effectively linearised and a different linearisation technique had to be applied.

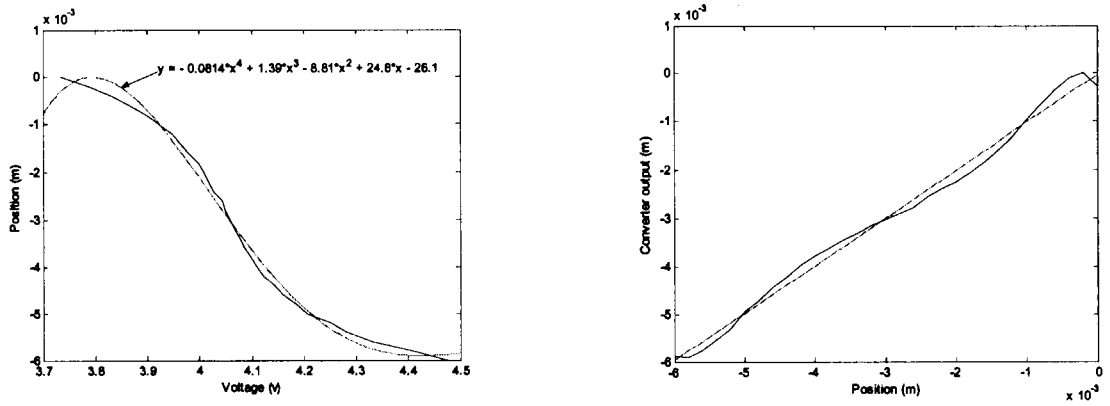

(a) Fitted polynomial (b) Linearity characteristic

Figure 3.7: Sensor linearisation

Look-up table interpolation was therefore implemented to linearise the sensor with satisfactory results as shown in Figure 3.8.

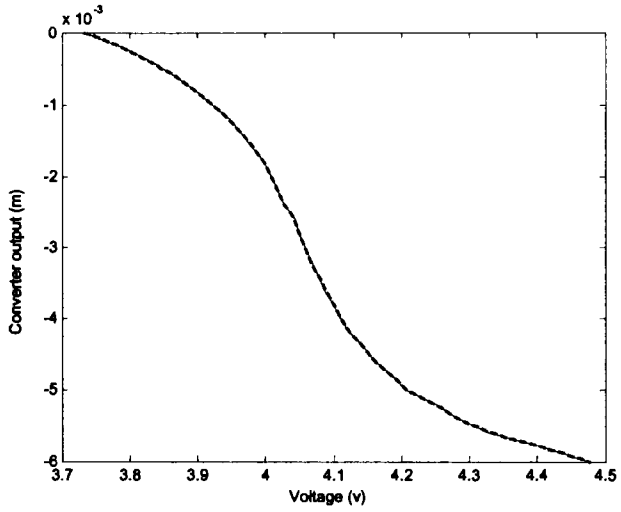

Figure 3.8: Comparison between measured sensor data and interpolation

3.2.3 Power amplifiers

An inductive sensor which is very susceptible to noise is used on the experimental model and therefore the decision was taken to use linear power amplifiers. Although linear amplifiers have low efficiency they emit less noise than switching amplifiers. Table 3.3 summarises the specifications of the power amplifier.

Table 3.3: Power amplifier specifications

Parameter	Specification
Rms current	3 A
Maximum voltage	50 V

Figure 3.9 shows the linear amplifier implemented in the system. The amplifier can be divided into an optical isolator, an error amplifier, a current sensing circuit and a current control element. The optical isolator was introduced into the system to protect the dSpace controller card from dangerous voltage spikes which might be generated by the power electronic circuit. The error amplifier compares the desired current to the current flowing through the coil of the electromagnet. The output of the error amplifier is the control signal for the power amplifier. The signal used to represent the current flowing through the coil of the electromagnet is generated as a voltage across a sense resistor and compared to the desired current. The current control element is a MOSFET operated in its linear region.

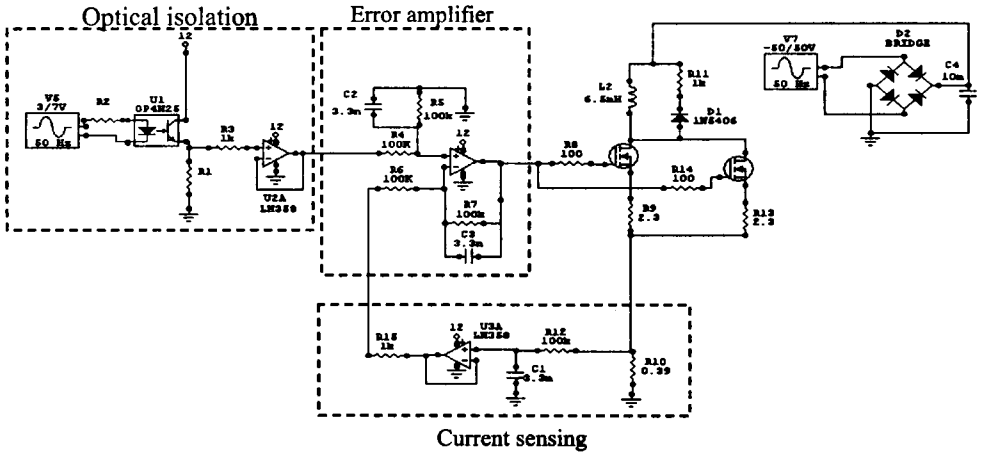

Figure 3.9: Power amplifier circuit [2]

- **Power amplifier identification**

The slewrate and bandwidth of the power amplifier directly influences the total response of the system therefore it has to be characterized. The power amplifier's negative slewrate was determined as -2100 A/s and the positive one as 82 A/s. The reason for the difference between the two flanks can be attributed to the design of the power amplifier. During the rising flank of the amplifier 50 V is applied across the actuator coil, but when the amplifier is switched off for the descending flank a spike of -450 V is applied across the coil due to the large resistance in the free wheeling path of the MOSFET, resulting in a high slewrate.

Figure 3.10(a) and Figure 3.10(b) show the two flanks of the amplifier with a peak to peak current reference of 1.9 A.

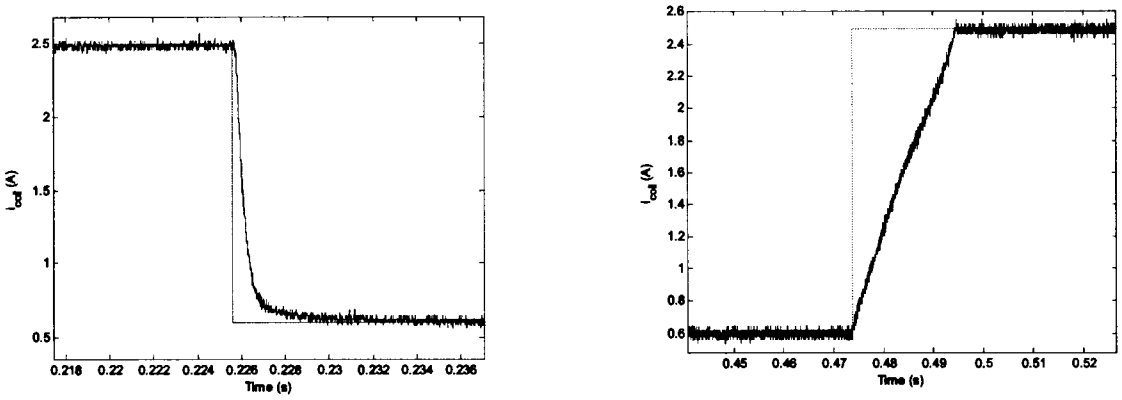

(a) Descending flank (b) Ascending flank

Figure 3.10: Power amplifier step response

3.2.4 Total system response

To obtain the total system response, the different system components were integrated and operated with a PD controller with the controller constants not yet optimised. The PD optimisation process is discussed in chapter 4. A 1 mm step input around the operating point was supplied to the system. This is a relatively large perturbation, but the system remained stable under these conditions proving it suitable for the study. This large perturbation was used to ensure that the nonlinear range of the system is covered. Figure 3.11 shows the step response of the system for a perturbation of 1000 μm.

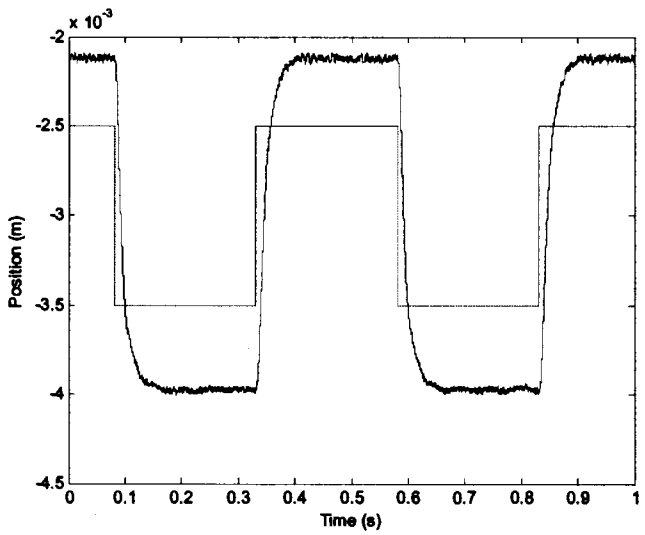

Figure 3.11: Total system practical step response for a 1 mm step input

3.3 Simulation model

3.3.1 Actuator

The actuator configuration is configured as illustrated in Figure 3.12 with x_1 the airgap of the top magnet and x_2 the airgap of the bottom magnet. The resultant force generated by the actuator is given by (2) with m the mass of the disc, x is the distance of the disc from the reference point, g the gravitational acceleration and F_{m1} and F_{m2} the magnetic control forces of the top and bottom electromagnets given by (3) and (4) respectively [22].

$$F_t = F_{m1} - F_{m2} - mg = m\ddot{x} \tag{2}$$

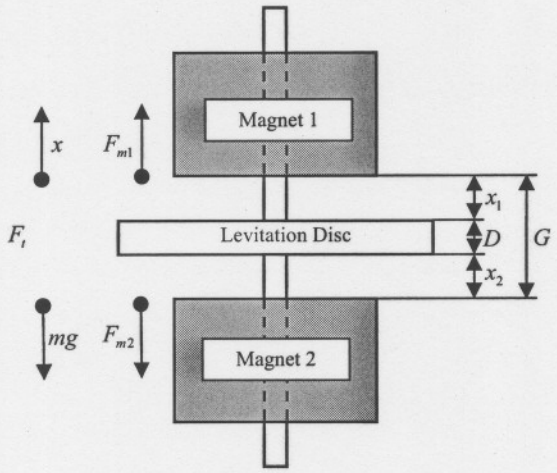

Figure 3.12: Actuator configuration

$$F_{m1} = k_m \frac{i_1^{\,2}}{x_1^{\,2}} \tag{3}$$

$$F_{m2} = k_m \frac{i_2^{\,2}}{x_2^{\,2}} \tag{4}$$

i_1 and i_2 are the currents that determine the forces exerted on the disk by the top and bottom magnets respectively. k_m is a magnetic force constant determined by the electromagnet characteristics. Assuming ideal current amplifiers, i_1 and i_2 can be replaced by u_{m1} and u_{m2} respectively. u_{m1} and u_{m2} are the control signals for the top and bottom magnets respectively. The acceleration of the mass can then be determined as shown in (5).

$$\begin{aligned} m\ddot{x} &= k_m \frac{u_{m1}^{\,2}}{|x_1|^2} - k_m \frac{u_{m2}^{\,2}}{|x_2|^2} - mg \\ \therefore \ddot{x} &= \frac{k_m}{m}\frac{u_{m1}^{\,2}}{|x_1|^2} - \frac{k_m}{m}\frac{u_{m2}^{\,2}}{|x_2|^2} - g \end{aligned} \tag{5}$$

The acceleration represents the basic AMB model for the simulation.

3.3.2 Power amplifiers

The linear power amplifier is modelled by a variable resistor as shown in Figure 3.13. The resistance is modelled as a function of the gate voltage applied to the MOSFET of the amplifier.

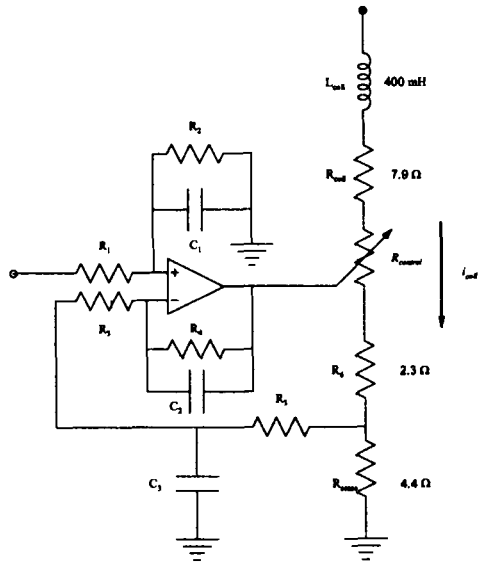

Figure 3.13: Model of linear power amplifier

Deriving a precise model of the power amplifier proved to be quite complex. A mathematical model of the power amplifier satisfying both the static and dynamic behaviour is derived.

In the steady state with a supply voltage at 50 V the value of $R_{control}$ is given by (6)

$$R_{control} = \frac{50}{i_{coil}} - R \tag{6}$$

with $R = R_{sense} + R_{coil} + R_6$.

To satisfy both the steady state and dynamic requirements the i_{coil} in (6) is intuitively replaced with a dynamic control variable; a scaled error signal of the error amplifier given by (7)

$$error = a \cdot i_{ref} - b \cdot i_{coil} \tag{7}$$

with a the gain of the reference signal and b the gain in the feedback loop. These gains are included to allow manipulation of the dynamic behaviour while satisfying steady state conditions of the PA.

To satisfy a steady state requirement of 1 % error, i_{ref} in (7) is replaced by $1.01 i_{coil}$ resulting in (8).

$$error = (1.01a - b) i_{coil} \tag{8}$$

error must however be equal to i_{coil} which results in

$$\begin{aligned} i_{coil} &= (1.01a - b) i_{coil} \\ 1 &= (1.01a - b) \\ \therefore b &= 1.01a - 1 \end{aligned} \tag{9}$$

A control law analogue to (6) is then defined by **Error! Reference source not found.**. In (6) i_{coil} is replaced by *error*.

$$\begin{aligned} R_{control} &= \frac{50}{error} - R \\ &= \frac{50}{a \cdot i_{ref} - b \cdot i_{coil}} - R \end{aligned} \tag{10}$$

By choosing one of the gains, the other can be determined using (9). The simulated response of the power amplifier can therefore be accurately matched to that of the practical amplifier.

Figure 3.14 shows the simulated response of the power amplifier for a 1.9 A pk-pk reference step. Both the falling and rising flanks of the power amplifier are shown in Figure 3.14.

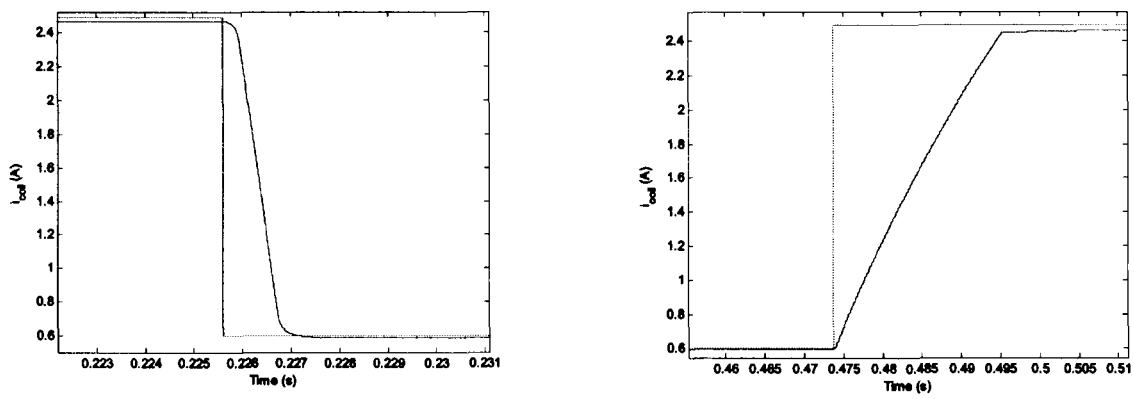

(a) (b)

Figure 3.14: Simulated (a) falling and (b) rising flanks of power amplifier

When compared to Figure 3.16 a remarkable correlation between the model and the actual response is evident.

3.3.3 Total system response

The step response given in Figure 3.15 was realised with the integrated system. The PD controller was not optimised and the results were used for model matching purposes.

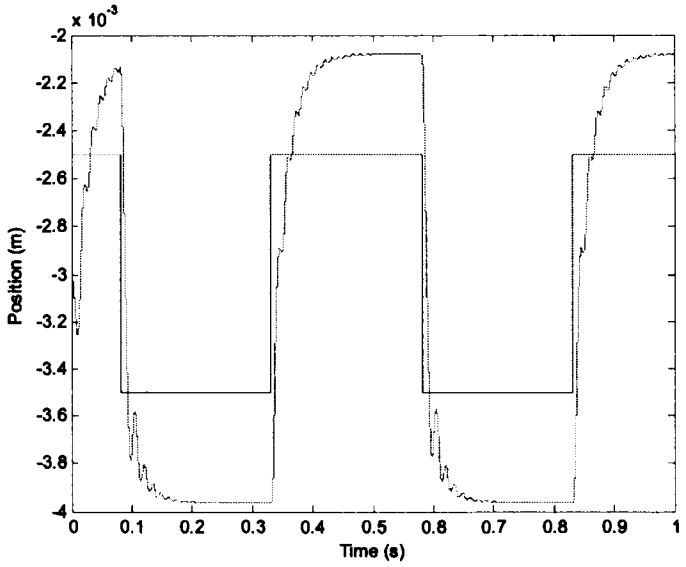

Figure 3.15: Total system simulation step response for a 1 mm step input point

3.4 Comparative evaluation

3.4.1 Power amplifier

Figure 3.16(a) shows the comparative response for the falling flank of the power amplifier for a 1.9 A pk-pk reference step. The response shows a slight inaccuracy between the simulated and practical result. This discrepancy does not have a noticeable influence on the total system response and is therefore adequate for the comparative study. Figure 3.16(b) shows a perfect correlation between the simulated and practical results.

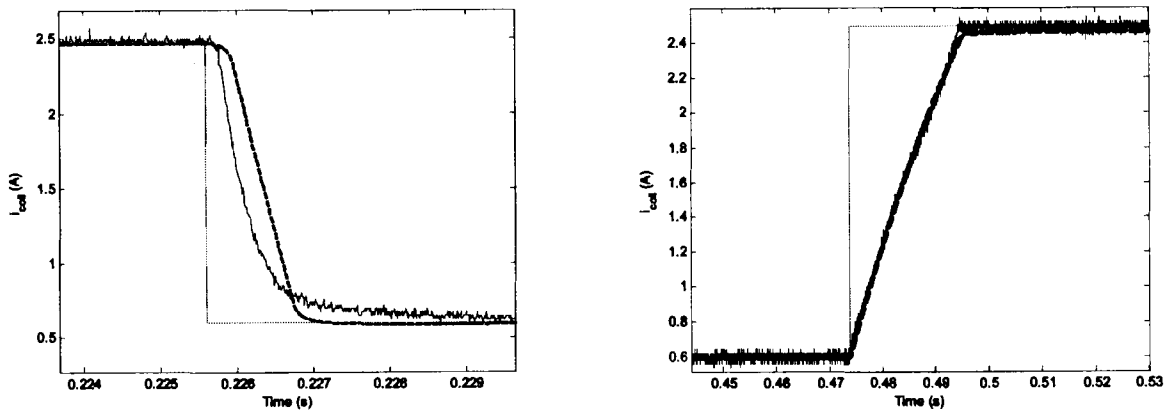

Figure 3.16: Comparative (a) falling and (b) rising flanks of power amplifier

3.4.2 Total system response

Figure 3.17 shows the close correlation between the simulated practical results of the integrated system. The remarkable results were achieved by closely matching the simulated response to the practical response of each component in the AMB system.

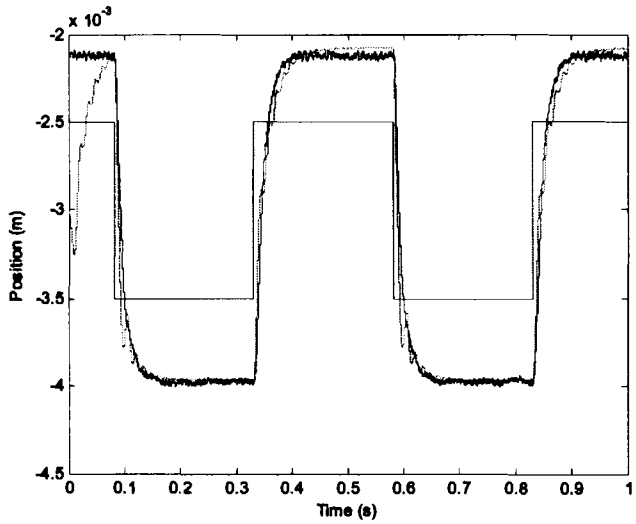

Figure 3.17: Comparative total system response

The close correlation between the simulated and practical response of the total system implies that the PD controller can be optimised in the simulation and implemented on the experimental system with equivalent results.

3.4.3 Matching of simulated and experimental results

An accurate simulation model is crucial in the design of an AMB system. To match the simulation with the practical system each component was considered individually. The sensor

displayed non-linear behaviour and was linearised by lookup-table interpolation. The two power amplifiers' transfer characteristics differed due to component variance and were compensated for by mapping the input-output relationship in dSPACE. The electromagnets were characterised and a value of 400×10^{-3} N.m^2/A^2 was calculated for k_m.

3.5 Conclusion

An existing experimental model was identified as the experimental platform and modified to increase its suitability for the comparative study. A simulation model of the experimental model was created to enable system optimisation and evaluation. The simulation model was accurately matched to the experimental model by individually matching the components of the simulated model to the experimental model. Total correlation between the two platforms was however very difficult due to certain model uncertainties. The simulation model nonetheless serves its purpose to obtain an initial approximation of the controllers.

Chapter 4

Linear Control

4.1 Introduction

Most physical systems show linear performance within some range of the variables. However, all systems ultimately become nonlinear as the variables are increased without limit. The question of linearity and the range of applicability must be considered for each system.

A system is defined as linear in terms of the system excitation $x(t)$ and response $y(t)$. When a system at rest is subjected to an excitation $x_1(t)$, it provides the response $y_1(t)$ and when the same system is subjected to the excitation $x_2(t)$, it provides the corresponding response $y_2(t)$. For a linear system the excitation $x_1(t)+ x_2(t)$ must result in the response $y_1(t)+ y_2(t)$ and is called the principle of superposition [4].

In addition to the principle of superposition, a linear system must also satisfy the property of homogeneity. This specifies that if the excitation $x(t)$, of a system is multiplied by a constant β, the response of the system must be the response to the input multiplied by the same constant β.

A linear system satisfies both the properties of superposition and homogeneity [4].

4.1.1 Linear model

The force (f) that an electromagnet exerts on a suspended body decreases quadratically with an increase in displacement and increases quadraticly with an increase of current through the coil as shown in Figure 4.1. These factors cause the poles of the system to lie in the right half s-plane and instantly destabilises the system.

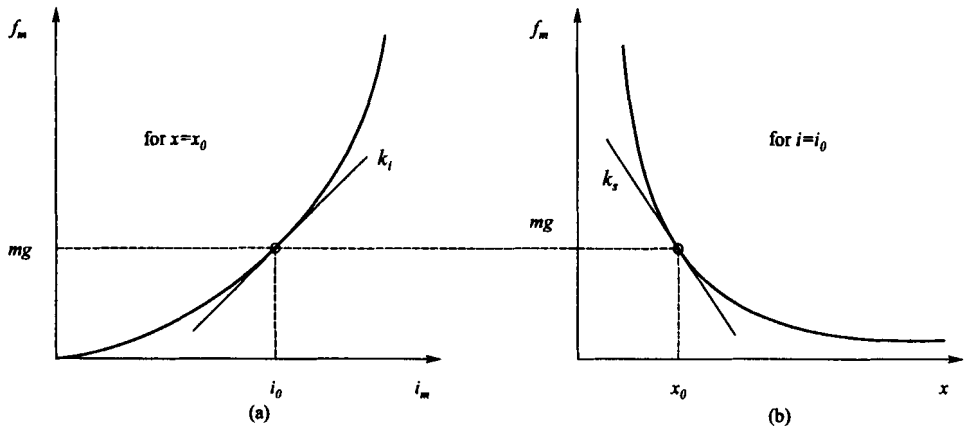

Figure 4.1: Magnetic force as a function of (a) current and (b) displacement

It is sufficient for linear AMB control design to consider only the slopes of the nonlinear force-current and force-displacement curves at the operating point. Figure 4.1(a) shows this linearisation of the force-current function. The slope of the force-current curve is called the force-current factor k_i and the unit of k_i is Newton/Ampère (N/A).

Figure 4.1(b) shows that the linearisation of the force-displacement function is carried out in the same way. The slope of the force-displacement function is called the force-displacement factor k_s and its unit is N/m or N/mm, which is the same as mechanical stiffness. All three variables, force, displacement and current have analogue definitions for the operating point, they are constant operating point values (mg, x_0, i_0) and variables (f, x, i) for deviations from the operating point. The resultant force in the operating point is zero by definition due to the equilibrium of forces. With these definitions, the total instantaneous force f as a function of displacement and current becomes a single linearised equation (5) around the operating point (11).

$$f(x,i) = k_s \cdot x + k_i \cdot i \tag{11}$$

This equation becomes less accurate as the distance from the operating point increases.

As shown in Figure 4.2 the axial AMB is operated in the differential driving mode. This means two counteracting magnets are used to generate positive and negative forces on the disc. The one magnet is driven by the sum of the bias current i_0 and the control current i_x, while the other one is

driven by the difference between them. With this configuration a linear force-current relation is achieved.

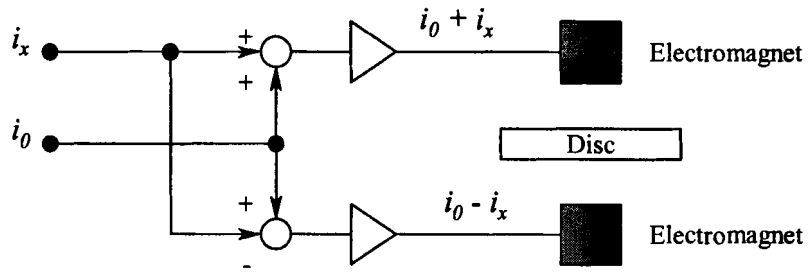

Figure 4.2: Differential driving mode

In (12) f_r is the difference between the forces of the top and bottom magnets of the axial AMB. The individual forces are obtained by substituting the current i with $(i_0 + i_x)$ in the top magnet and $(i_0 - i_x)$ in the bottom one. The displacement x is substituted with $(x_0 + x)$ and $(x_0 - x)$ in the top and bottom magnet force equations respectively.

$$\begin{aligned} f_r &= f_{top} - f_{bottom} \\ &= k\left(\frac{(i_0 + i_x)^2}{(x_0 - x)^2} - \frac{(i_0 - i_x)^2}{(x_0 + x)^2}\right) \end{aligned} \tag{12}$$

with k the electromagnet constant.

If (12) is linearised and simplified with respect to $x << x_0$ (13) is obtained which is the same result as in (11). The assumption made in the simplification is that the electromagnet constant k is the same for both magnets.

$$\begin{aligned} f_r &= \frac{4k\,i_0}{x_0^{\,2}} i_x + \frac{4k\,i_0^{\,2}}{x_0^{\,3}} x \\ &= k_i\, i_x + k_s\, x \end{aligned} \tag{13}$$

The linear system block diagram of the axial AMB is shown in Figure 4.3. The controller shown in the diagram is a PD controller. The system with the PD controller serves as the basis for the comparative study and is therefore in the characterisation and linearisation of the system. The

control signal, u, of the PD controller is obtained from the error signal, e. The control signal contains a term proportional to the error of the process and one proportional to the rate of change in the error. By adjusting the gains, k_p and k_d, of these terms, the steady state error and dynamic response of the position of the disc can be adjusted. This in turn influences the equivalent stiffness and equivalent damping of the AMB system.

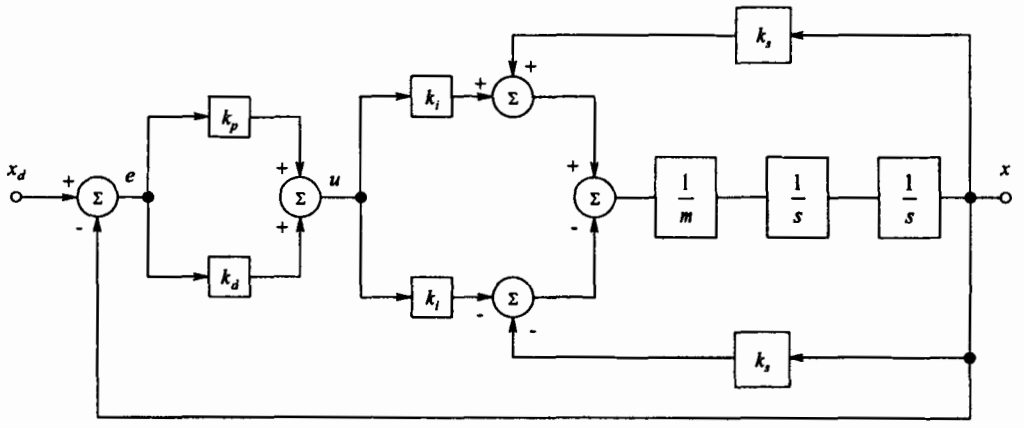

Figure 4.3: Linear system block diagram

The signal flow diagram shown in Figure 4.4 is derived from the block diagram in Figure 4.3.

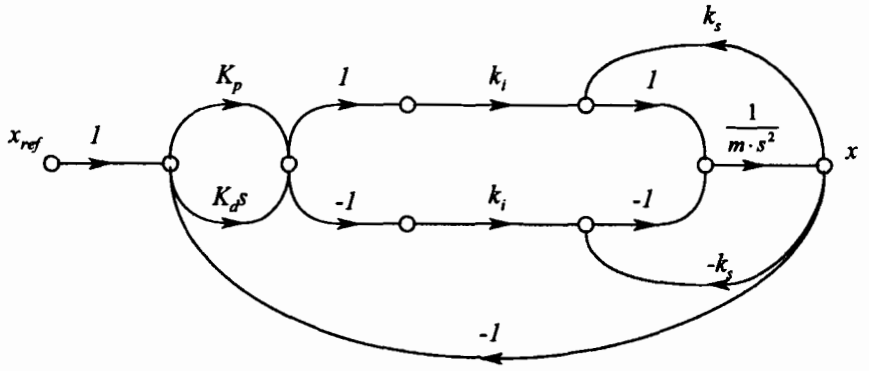

Figure 4.4: Signal flow diagram

From the signal flow diagram in Figure 4.4 the forward paths connecting the input to the output are:

$$P_1 = \frac{k_p k_i}{ms^2},\ P_2 = \frac{k_d k_i s}{ms^2} = \frac{k_d k_i}{ms}$$
$$P_3 = \frac{k_p k_i}{ms^2},\ P_4 = \frac{k_d k_i s}{ms^2} = \frac{k_d k_i}{ms} \qquad (14)$$

Six loops are identified:

$$L_1 = \frac{k_s}{ms^2},\ L_2 = \frac{k_s}{ms^2},\ L_3 = \frac{-k_p k_i}{ms^2}$$
$$L_4 = \frac{-k_d k_i}{ms^2},\ L_5 = L_3,\ L_6 = L_4 \tag{15}$$

Loops L_1 through to L_6 touches, therefore the determinant is:

$$\Delta = 1 - (L_1 + L_2 + L_3 + L_4 + L_5 + L_6) \tag{16}$$

The cofactor of each forward path is evaluated by removing the loops that touch that specific path from the determinant. Therefore the cofactors are:

$$\Delta_1 = \Delta_2 = \Delta_3 = \Delta_4 = 1 \tag{17}$$

The system transfer function is obtained using (18).

$$\begin{aligned} T &= \frac{P_1 \cdot \Delta_1 + P_2 \cdot \Delta_2 + P_3 \cdot \Delta_3 + P_4 \cdot \Delta_4}{\Delta} \\ &= \frac{\dfrac{2k_p k_i}{ms^2} + \dfrac{2k_d k_i}{ms}}{1 - \left(\dfrac{2k_s}{ms^2} - \dfrac{2k_p k_i}{ms^2} - \dfrac{2k_d k_i}{ms} \right)} \\ &= \frac{2k_p k_i + 2k_d k_i s}{ms^2 + 2k_d k_i s + (2k_p k_i - 2k_s)} \end{aligned} \tag{18}$$

The resulting characteristic equation for this system is as given by (19).

$$\begin{aligned} q(s) &= s^2 + \frac{2k_d k_i}{m} s + \frac{2k_p k_i - 2k_s}{m} \\ &= s^2 + \frac{b_{eq}}{m} s + \frac{k_{eq}}{m} \end{aligned} \tag{19}$$

The result in (19) illustrates equivalence to a spring-mass-damper system, which implies that the AMB system with a single controller and two electromagnets will display dynamic behaviour equivalent to that of a spring-mass-damper system. The equivalent damping for this system is derived from (19) as

$$b_{eq} = 2k_d k_i \tag{20}$$

and the equivalent stiffness as

$$k_{eq} = 2k_p k_i - 2k_s \tag{21}$$

The results obtained in (20) and (21) can now be used to design a simple PD controller which will result in a stable system with the desired equivalent stiffness and damping values.

4.2 PD control

The first goal of control design is to stabilize the contact free equilibrium. The PD controller has to provide a restoring force similar to that of a spring suspension and a damping has to attenuate oscillations. This is achieved by exerting forces proportional to displacement and velocity of the suspended body. By specifying the equivalent stiffness and equivalent damping of the AMB, the k_d and k_p values of the PD controller can be determined by using (20) and (21) respectively.

4.2.1 Results

Due to modelling uncertainties it was extremely difficult to design a controller in the conventional method with a predetermined stiffness and damping. The method followed to implement the controller was to intuitively optimise the controller for different step inputs. This process is demonstrated by the flow diagram in Figure 4.5

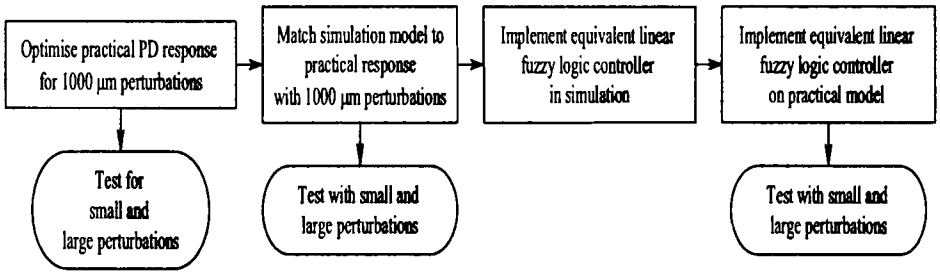

Figure 4.5: Methodology flow diagram

The process followed for the study was to firstly simulate the different controllers in MATLAB® and to intuitively adjust the control parameters for the best response. The PD controller was implemented practically via dSpace and optimised for a 1000 µm step response around the operating point. The PD simulation was matched to the practical system response for a 1000 µm step and was used as the basis for the comparative study. Two additional responses were measured to determine the robustness of the controller. The additional measurements were taken for a step response of 200 µm 1500 µm respectively.

The equivalent stiffness, k_{eq} of the system was determined by suspending the steel disc with the PD controller. This position was recorded as position 1, a disturbance force ($f_{disturb}$) of 3 kg was

introduced to the system and the position of the disc under the influence of the disturbance force recorded as position 2. The difference in position is illustrated in Figure 4.6 and the equivalent stiffness of the system determined using (22).

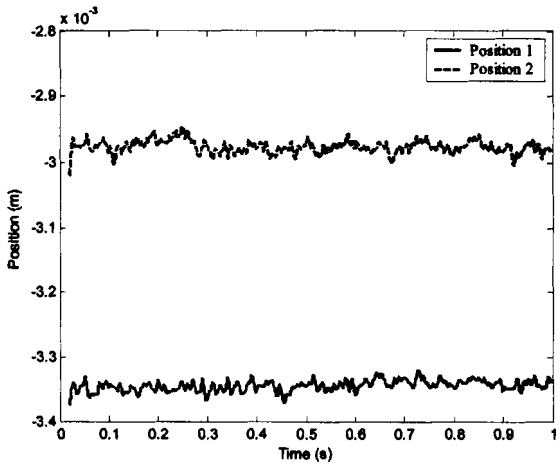

Figure 4.6: Position deviation for equivalent stiffness calculation

$$\begin{aligned} k_{eq} &= \frac{f_{disturb}}{\Delta x} \\ &= \frac{3 \cdot 9.81}{(-0.00309 - -0.00334)} \\ &= 79.8 \text{ kN/mm} \end{aligned} \tag{22}$$

Figure 4.9(b) shows that the AMB system is an overdamped system and by using the characteristic equation given in (19), the damping of the system can be determined from (23). Equation (22) represents the pole positions of the system and it is assumed that the pole nearest the origin is dominant and therefore will be the only pole investigated. The time constant (τ) of the system is determined as 15.3 ms from Figure 4.7. The equivalent damping of the system is determined in (25) as 1351.5 N.s/mm.

$$P_1, P_2 = \frac{-b_{eq} \pm \sqrt{b_{eq}^{\,2} - 4 \cdot m \cdot k_{eq}}}{2 \cdot m} \tag{23}$$

$$-\frac{1}{\tau} = \frac{-b_{eq} + \sqrt{b_{eq}^{\,2} - 4 \cdot m \cdot k_{eq}}}{2 \cdot m} \tag{24}$$

$$-\frac{1}{15.3\times10^{-3}}=\frac{-b_{eq}+\sqrt{b_{eq}{}^{2}-4\cdot2\cdot79.792\times10^{3}}}{2\cdot2}$$
$$b_{eq}=1351.5\ \text{N.s/mm} \tag{25}$$

Figure 4.7(a) shows k_p the optimised simulation result for a 1 mm perturbation around the operating point of 3 mm. The value for the controller was determined as 864 and the k_d value as 10. These values were determined by intuitively optimising the practical step response on the practical model which is shown in Figure 4.7(b).

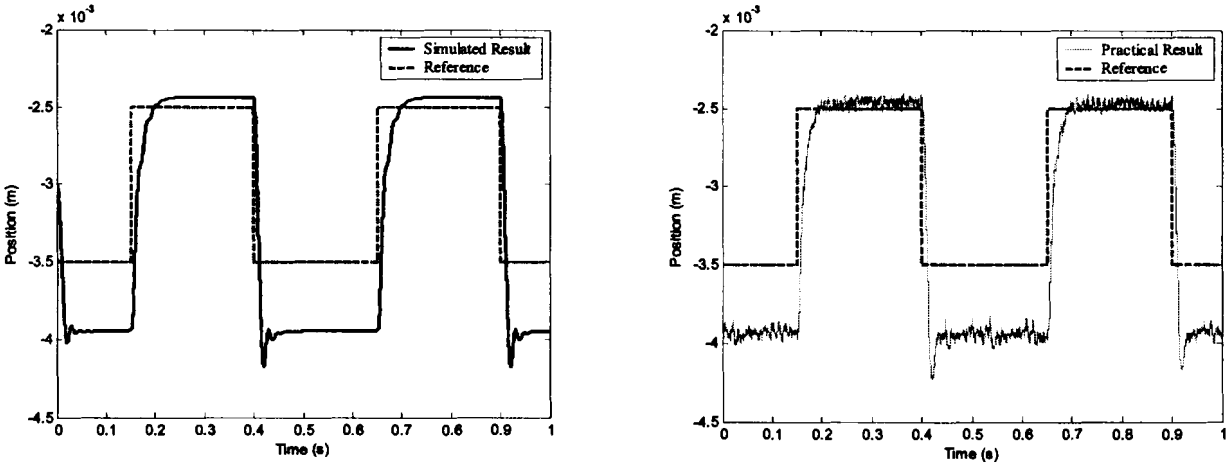

(a) (b)

Figure 4.7: PD controller results for optimised perturbation (1000 μm)

Figure 4.8 shows the correlation between simulated and practical results to a step response. From this result it is evident that the dynamic responses of the two results correspond remarkably well.

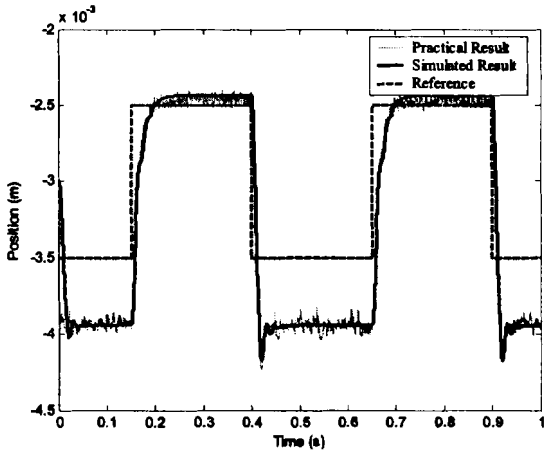

Figure 4.8: Comparative simulation and practical results (1000 μm)

The undershoot observed in the results can be attributed to the different slew rates between the rising and falling flanks of the power amplifiers as was explained in paragraph 3.2.3.

Figure 4.9 shows the simulated and practical results for the system with the 200 μm perturbation around the operating point. With the small perturbation it is clear that the response has deteriorated somewhat. The reason for the poorer response is that the system was optimised for large perturbations around the operating point and the controller constants are not suited for small perturbations.

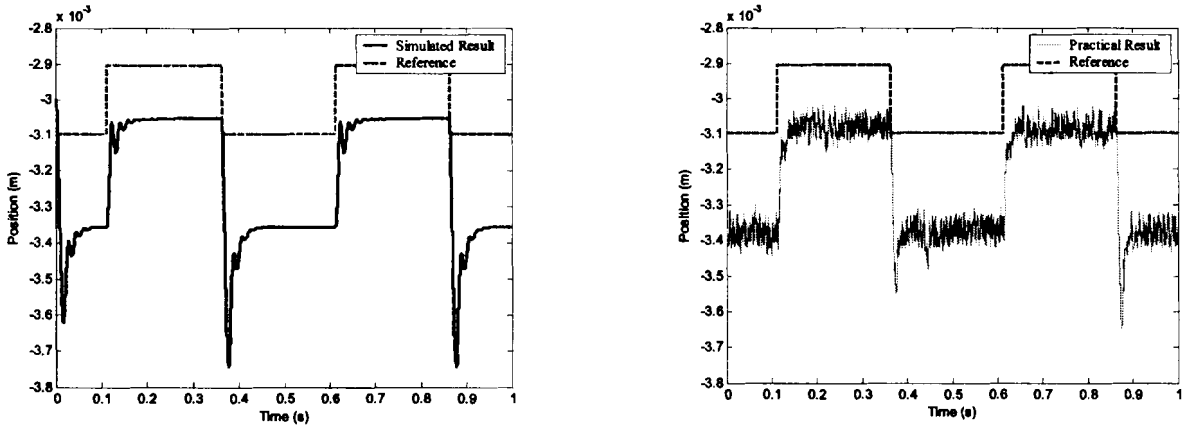

(a) (b)

Figure 4.9: PD controller results for small perturbation (200 μm)

The comparison between the simulated and practical results shown in Figure 4.10 still shows remarkable correlation for the small perturbation. This indicates that the dynamics of the simulated model closely resembles that of the practical system.

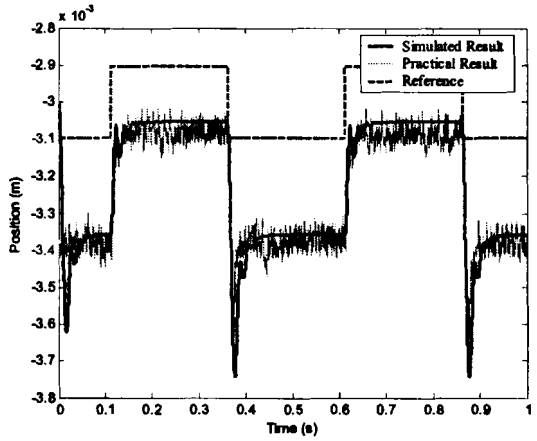

Figure 4.10: Comparative simulation and practical results (200 μm)

To determine the robustness and for purposes of comparison a step response for a large perturbation of 1500 μm was also taken. Figure 4.11 demonstrates that the performance of the controller for this setup is very good and suggests that this basis is suitable for the comparative study.

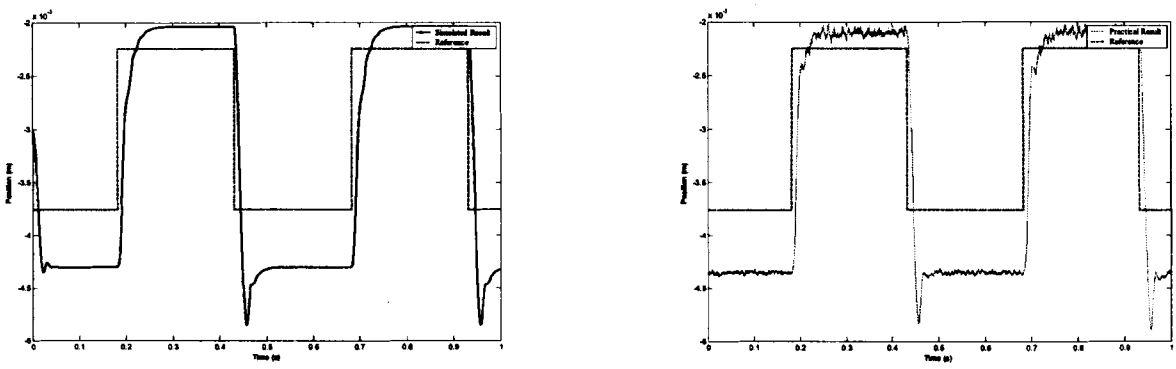

(a) (b)

Figure 4.11: PD controller results for large perturbation (1500μm)

From Figure 4.12 it is once again clear that the simulated and practical results show very good correlation. This indicates that the relevant dynamics of the practical model are included in the simulation model.

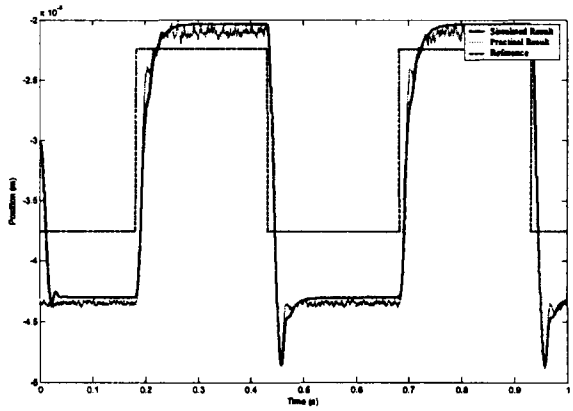

Figure 4.12: Comparative simulation and practical results (1500 μm)

4.3 Fuzzy logic control

Lotfi A. Zadeh, a professor of UC Berkeley in California, known as the founder of fuzzy logic observed that conventional computer logic was incapable of manipulating data representing subjective or vague human ideas. Fuzzy logic was therefore designed to allow computers to determine the difference between data with shades of gray, similar to the process of human

reasoning. In 1965, Zadeh published his seminal work "Fuzzy Sets" which described the mathematics of fuzzy set theory, and by extension fuzzy logic. This theory proposed making the membership function operate over the range of real numbers [0, 1]. Fuzzy logic was then introduced to the world.

The word "fuzzy" is defined as lacking in clarity or definition by the Webster's online dictionary. In contrast, in the technical sense, fuzzy systems are precisely defined systems, and fuzzy control is a precisely defined method of non-linear control. The main goal of fuzzy logic is to mimic "human-like" reasoning [12].

4.3.1 Fuzzy logic background

Most if not all of the physical processes are non-linear and to model them, a reasonable amount of approximation is necessary. For simple systems, mathematical expressions give precise descriptions of the system behaviour. For complex systems fuzzy reasoning provides a way to understand the system behaviour by relying on approximate input-output approaches. The underlying strength of fuzzy logic is that it makes use of linguistic variables rather than crisp numerical variables to represent imprecise data.

"Fuzzy systems are knowledge-based or rule-based systems". Specifically, the key components of a fuzzy system's knowledge base are a set of IF-THEN rules obtained from human knowledge and expertise. The fuzzy systems are multi-input-single-output mappings from a real-valued vector to a real-valued scalar. This can be implemented using one of the following methodologies [12]:

a) Pure fuzzy logic systems
b) Takagi-Sugeno fuzzy systems
c) Fuzzy systems with fuzzifier and defuzzifier

The methodology used in this study is the fuzzy system with fuzzifier and defuzzifier and a block diagram of the topology is given in Figure 4.13.

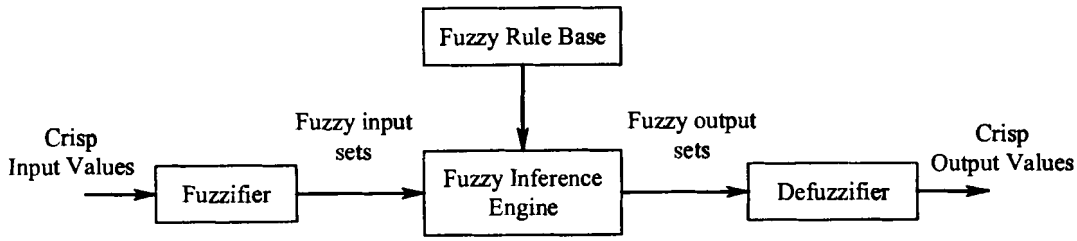

Figure 4.13: Fuzzy system with fuzzifier and defuzzifier

The starting point in the construction of a fuzzy logic system is the creation of a knowledge base in the form of *if-then* rules, shown as the fuzzy rule base in Figure 4.13. These rules can either be provided by a human expert or be inferred from measured data.

A fuzzifier is used to convert real crisp input values into fuzzy input sets, while a defuzzifier is used to transform fuzzy output sets into crisp output values. The difference between a real set and a fuzzy set, is that a real set has a well defined boundary. This means that an element is either included in or excluded from the set, while the boundary of a fuzzy set is not well defined and for certain elements of the set there is a gradual transition from exclusion to inclusion. This principle is demonstrated in Figure 4.14.

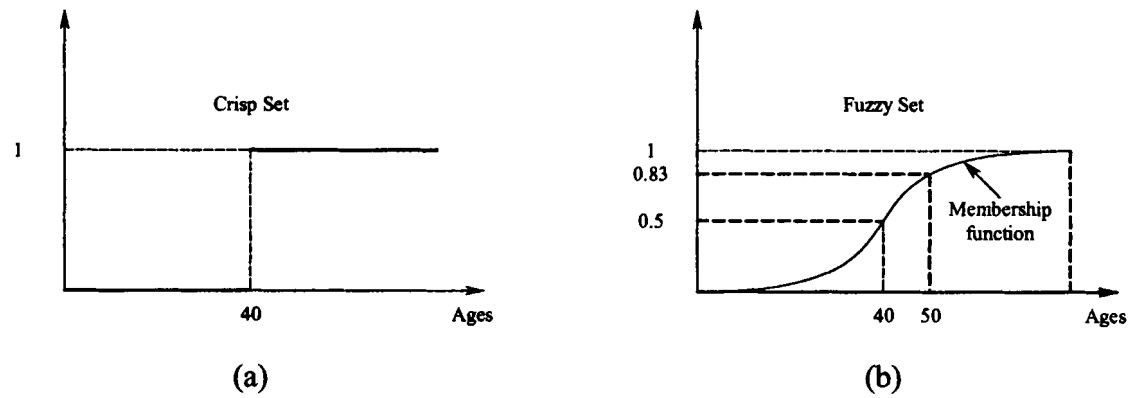

Figure 4.14: Fuzzy set demonstration

In Figure 4.14 both the diagrams represent a set of old age. In Figure 4.14(a) a person can be member of the crisp set with an age higher than 40 or be excluded from the set with an age smaller than 40. In Figure 4.14(b) all persons are members of the fuzzy set with a varying degree. The membership can vary between 0 (non-membership) and 1 (full-membership).

Therefore a person with the age of 40 will have a membership of 0.5 to fuzzy set of old age and as the age increases so does the membership.

Formally, a fuzzy set A is defined by a set of ordered pairs, a binary relation,

$$A = \{(x, \mu_A(x)) \mid x \in A, \mu_A(x) \in [0,1]\} \tag{26}$$

where $\mu_A(x)$ is a function called a membership function and $\mu_A(x)$ specifies the grade or degree to which any element x belongs to the fuzzy set A. (26) associates each element x in A with a real number $\mu_A(x)$ in the interval [0, 1] which is assigned to x. Larger values of $\mu_A(x)$ indicate higher degrees of membership [13].

A fuzzy set is characterised by a membership function of which the value ranges between 0 and 1. It is usually decided from human expertise and observations made and it can be either linear or nonlinear. Its choice is critical for the performance of the fuzzy logic system since it determines all the information contained in a fuzzy set.

A fuzzy rule base is a collection of fuzzy IF-THEN rules in the form:

$$R^{(l)} : IF\ x_1\ is\ F_1^l\ and.....and\ x_n\ is\ F_n^l,\ THEN\ y\ is\ G^l \tag{27}$$

where F_1^l and G^l are fuzzy sets in $U_i \subset R$ and $V \subset R$ respectively with U and V the input and output universes of discourse respectively. $\mathbf{x} = (x_1,.....x_n)^T \in U_1 \times .....U_n$ and $y \in V$ are linguistic variables. Let M be the number of fuzzy IF-THEN rules in the form of (27) in the fuzzy rule base, that is l = 1,2,....,M in (27). The x and y are the input and output of the of the fuzzy logic system respectively.

The fuzzy rule base is the heart of the fuzzy logic system in the sense that the other components (fuzzy inference engine, fuzzifier and defuzzifier) are all used to interpret these rules and make them useable for specific problems [14].

In a fuzzy inference engine, fuzzy principles are used to combine the fuzzy rule base into a mapping from fuzzy input sets in $U_1 \times .... \times U_n$ to output fuzzy sets in V.

The mapping then provides a basis from which decisions can be made, or patterns discerned. The process of fuzzy inference involves all of the pieces that are described in the previous sections: membership functions, fuzzy logic operators, and if-then rules [15].

4.3.2 Controller design

To make a sensible comparison between a classical PD controller and an equivalent fuzzy logic controller fuzzy logic controller has to be designed to emulate the response of the PD controller. It was expected that the equivalent fuzzy logic controller would have a larger operating range in comparison to the classical PD controller and being able to emulate the optimized response of a PD controller it is logical that a fuzzy logic controller is at least equivalent, if not superior to a classical controller.

A linear controller can be seen as a subset of a fuzzy logic controller and therefore it is possible to design an equivalent fuzzy logic controller by using the linear optimised PD controller as a starting point for the design of the linear fuzzy logic controller.

The input-output mapping for a linear controller is a weighted sum of the inputs where:

$$y = c_1 \cdot x_1 + ... + c_n x_n \tag{28}$$

The fuzzy controller function $y = f(x)$ can mimic a linear controller if the following criteria are met [16].

1. The membership functions of the input fuzzy sets must be triangularly shaped and normal.
2. The fuzzy sets for each input must form a fuzzy partition as given in (26).
3. The fuzzy rule base is complete.
4. The product operator must be used for conjunction in the premises of the fuzzy rules.
5. The sum operator must be used for aggregation and the or connective.
6. Crisp consequents must be considered for the individual fuzzy rules and their choice made in accordance to the linear controller equation.
7. The centroid defuzzification method must be used.
8. The output membership functions must be singletons.

With all the above criteria met the control surface for the fuzzy controller becomes linear as shown in Figure 4.15. A fuzzy controller equivalent to a classical PD controller can be derived by determining the gains as shown in Figure 4.16.

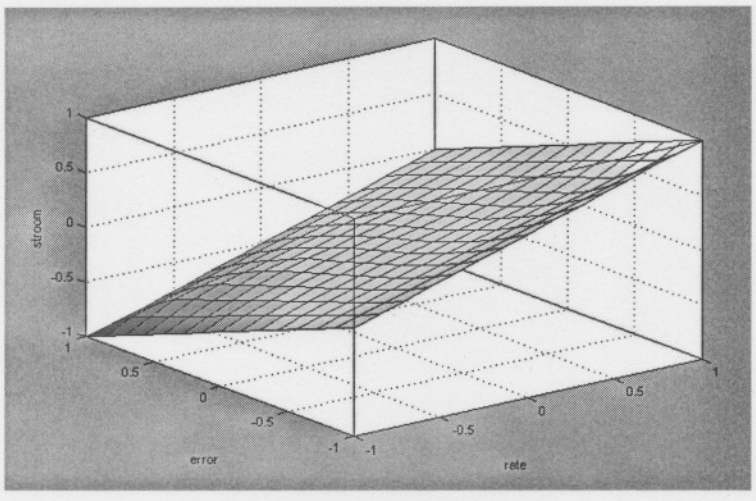

Figure 4.15: Linear control surface

To realise a linear fuzzy logic controller equivalent to the implemented PD controller the two gains, K_p and K_d, used in the conventional PD controller have to be transferred to three the fuzzy PD (FPD) controller gains (*GE, GR* and *GU*) [16].

The FPD controller emulates the PD controller as shown in (29).

$$\begin{aligned} u_1 &= K_p \cdot e + K_d \cdot \dot{e} \\ &= \left[GE \cdot e + GR \cdot \dot{e}\right] \cdot GU \\ &= GU \cdot GE \cdot e + GU \cdot GR \cdot \dot{e} \end{aligned} \tag{29}$$

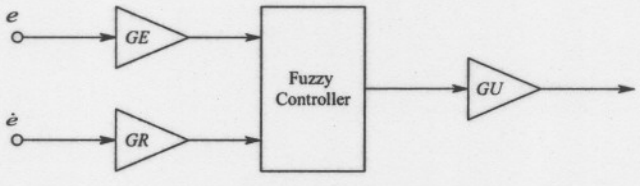

Figure 4.16: Equivalent fuzzy PD controller

Comparing the FPD gains to those of the PD controller the relations in (30) and (31) can be derived.

$$GE = \frac{K_p}{GU} \tag{30}$$

$$GR = \frac{K_d}{GU} \tag{31}$$

By using the relations in (30) and (31) and choosing *GU* as 20, *GE* was determined as 43.2 and *GR* as 0.5. *GU* was chosen as 20 to ensure that the entire output range of the controller can be achieved.

The controller designed above was implemented on the practical system, but it was obvious that the two controllers did not completely correlate as shown in Figure 4.17.

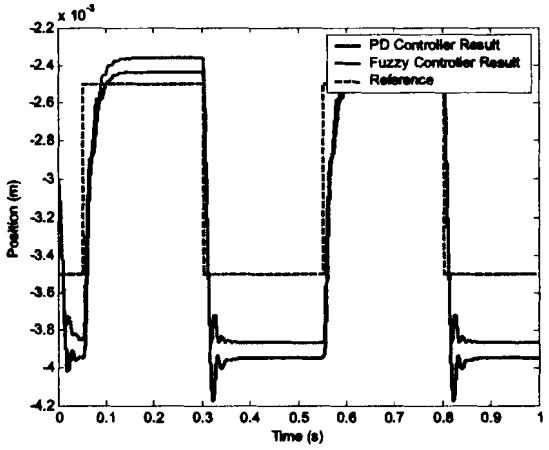

Figure 4.17: Comparison for calculated gain setup

To get the fuzzy controller to mimic the PD controller the input gains to the fuzzy controller were individually set to correspond with the input-output mapping of the PD controller. From the results achieved with the PD controller simulation, it is sufficient to use the simulation to obtain the gains of the fuzzy controller. This was done by firstly choosing the output gain (*GU*) large enough to ensure that the entire output range can be achieved. The value chosen for *GU* is therefore kept at 20. Both the derivative gain of the PD controller (K_d), as well as the derivative gain for the fuzzy controller (*GR*) was then set to zero and the error gain (*GE*) of the fuzzy controller was adjusted until the input-output mappings of the two controllers corresponded. By doing this the controllers are matched to produce similar steady state errors. The value for *GE* was determined as 126.86 in this manner.

To achieve similar transient dynamics, the derivative gain of the PD controller was set up with the optimised settings and a step response was taken. The fuzzy controller derivative gain *GR*

was then adjusted to achieve the best correlation between the two transients and was found to be 1.45. The comparative results of the simulation with this setup are given in Figure 4.18. It is evident from these results that a linear fuzzy logic controller that completely emulates a linear PD controller can be realised. The results of the FPD controller lies on top of the results of the PD controller in Figure 4.18.

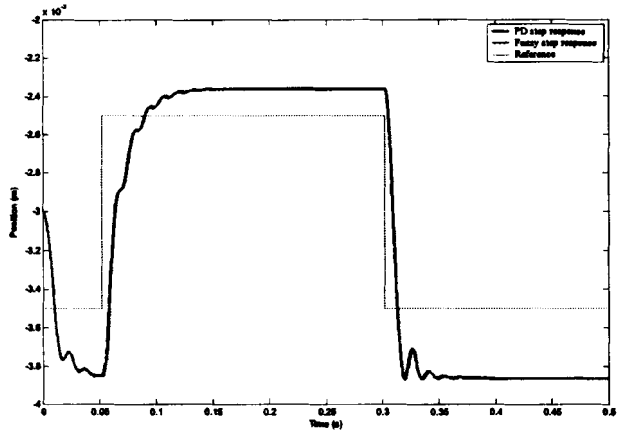

Figure 4.18: Comparison for correlated gain setup

4.3.3 Results

The equivalent stiffness and damping of the system with the fuzzy controller was determined in a similar fashion to that of the PD controller.

The position deviation for the 3 kg disturbance force is shown in Figure 4.19.

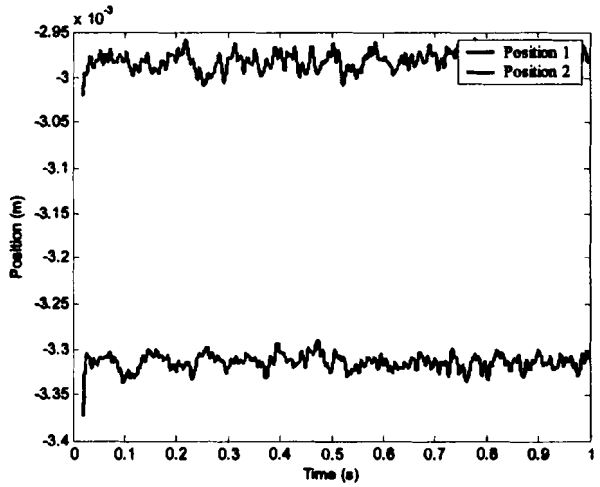

Figure 4.19: Position deviation for determination of stiffness

From this deviation the equivalent stiffness of the system is determined with (32) and found to be within 10 % of the stiffness of the PD controlled system. The difference in stiffness is due to the sensor drift observed in the system, making perfect correlation to the practical system very difficult.

$$k_{eq} = \frac{f_{disturb}}{\Delta x} = \frac{3 \cdot 9.81}{(-0.00331 - -0.00298)} \quad 88.635\,\text{kN/m} \tag{32}$$

The equivalent damping of the system was once again determined from the time constant of the step response which is exactly the same as that of the PD controller system. This perfect correlation is due to the fact that the damping of the system was determined from the simulated results which were adjusted for perfect correlation.

Figure 4.20(a) shows the simulation for the equivalent fuzzy logic controller for the optimised perturbation while Figure 4.20(b) shows the practical results.

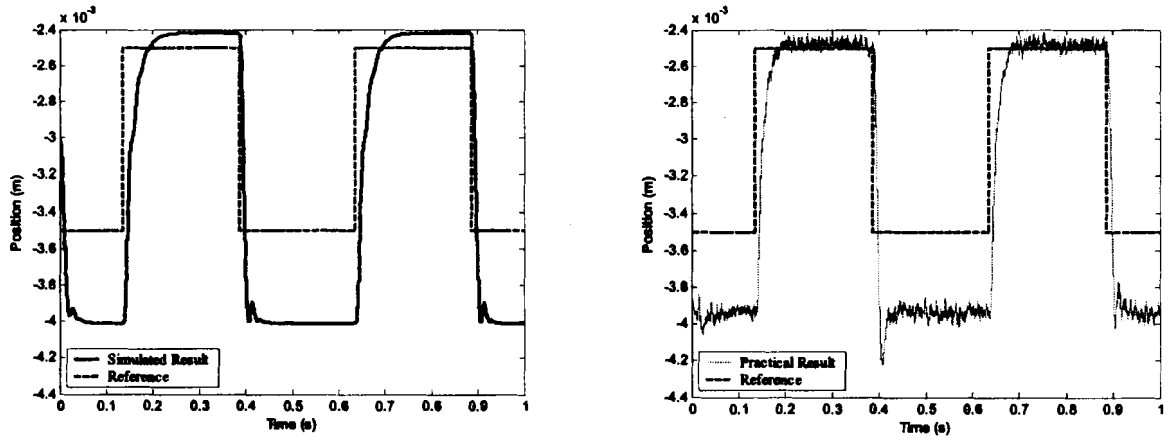

(a) (b)

Figure 4.20: Fuzzy controller results for optimised perturbation (1000μm)

Figure 4.21 presents the comparison between the practical and simulated responses for the 1000 μm perturbation. The two responses correlate incredibly well except for a small steady state error, which can once again be attributed to thermal drift in the sensor.

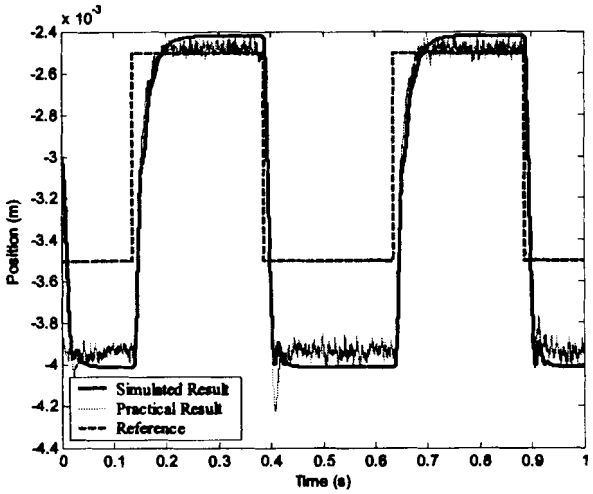

Figure 4.21: Comparative simulation and practical results (1000 μm)

Figure 4.22 shows the simulated and practical results for the system with the 200 μm perturbation around the operating point.

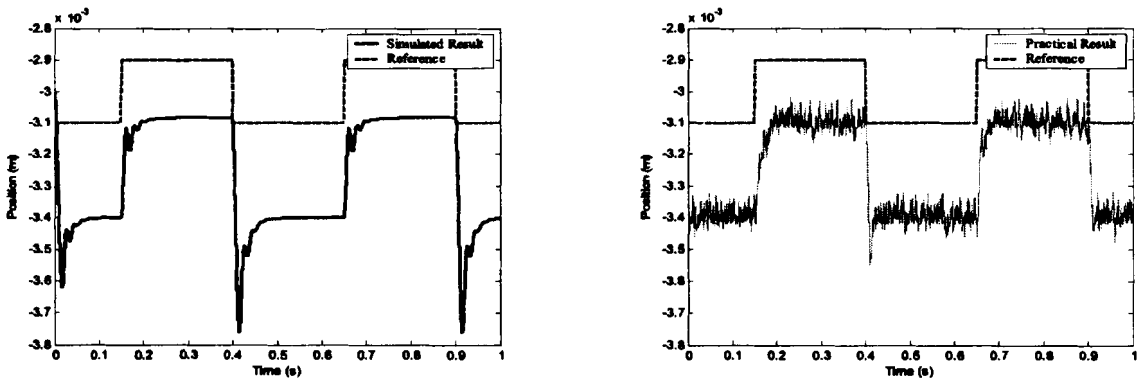

(a) (b)

Figure 4.22: Fuzzy controller results for small perturbation (200 μm)

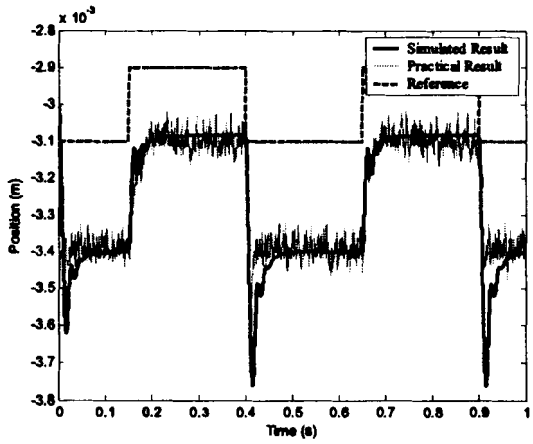

Figure 4.23: Comparative simulation and practical results (200 μm)

Figure 4.23 represents the comparison between the simulated and practical results for the system with the small perturbation. These results compare very well except for the undershoot, which does not repeat in both the steps of the practical result. This is due to the noise encountered in the system.

Figure 4.25 shows the FPD controller results of the system for the large perturbation.

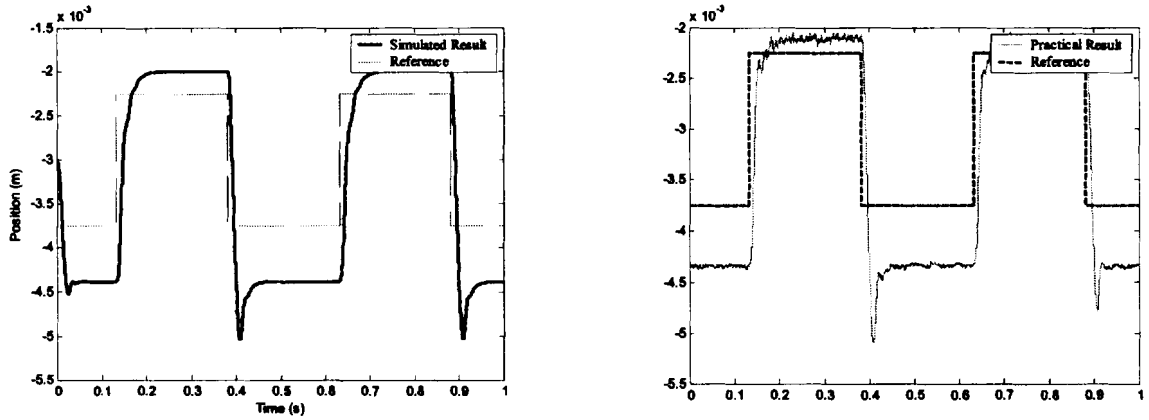

(a) (b)

Figure 4.24: Fuzzy controller results for large perturbation (1500 μm)

Figure 4.25 compares the simulated and practical results for the large perturbation. These results are once again impressive.

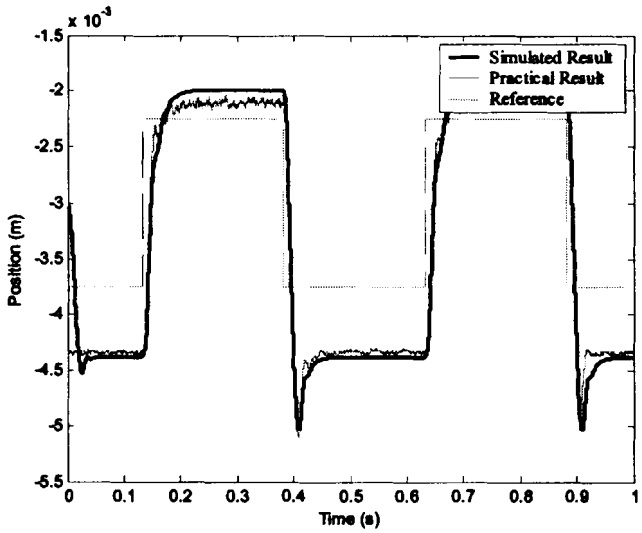

Figure 4.25: Comparative simulation and practical results (1500 μm)

4.4 Controller comparison

The equivalent stiffness and damping of the two linear controllers are shown in Table 4.1.

Table 4.1: Performance comparison of linear controllers

Performance comparison of linear controllers		
	PD controller	Fuzzy logic controller
Stiffness	79.8 kN/m	88.6 kN/m
Damping	1351.5 N.s/m	1351.5 N.s/m

This comparison already shows a remarkable resemblance. To be sure that the two controllers correlate both the simulated and practical results are compared for the three perturbations. This will determine whether the different controllers have the same response over the same operating range.

4.4.1 Simulation comparison

To determine the correlation between the linear PD controller and linear fuzzy logic controller the step responses for the three perturbations were compared. In all of the results nearly perfect correlation was displayed as illustrated in Figure 4.26 through to Figure 4.28.

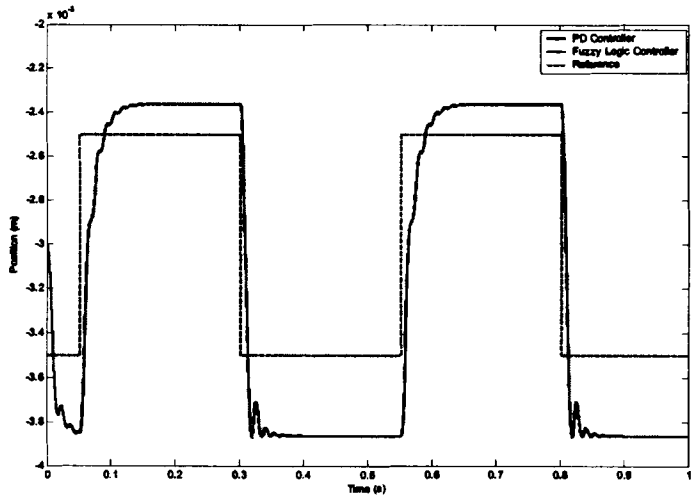

Figure 4.26: Simulation comparison for optimised perturbation (1000 μm)

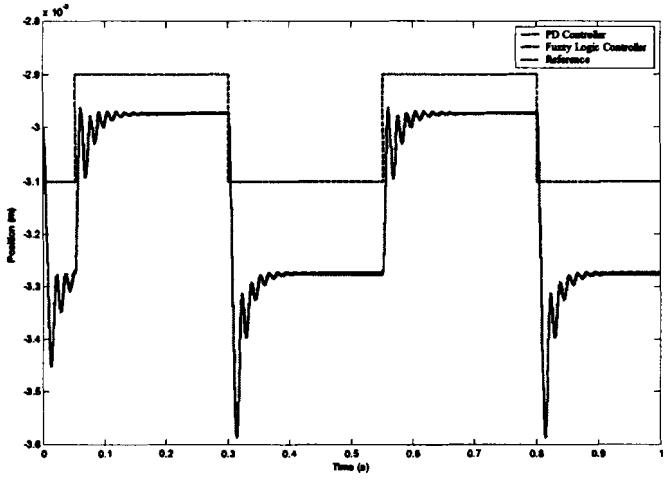

Figure 4.27: Simulation comparison for small perturbation (200 μm)

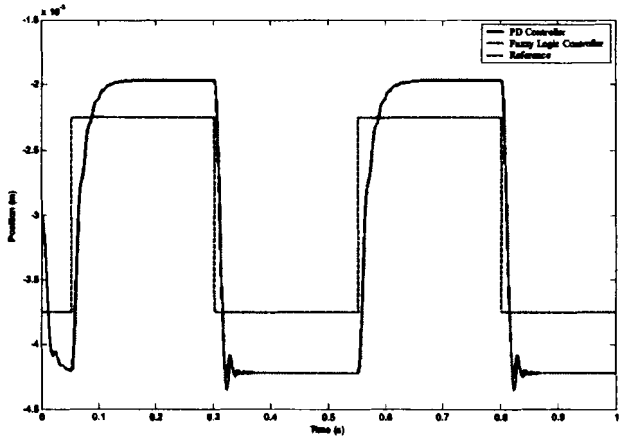

Figure 4.28: Simulation comparison for large perturbation (1500 μm)

4.4.2 Experimental comparison

The experimental comparisons between the two linear controllers were also made for the three different perturbations. Once again the responses correlated remarkably well as seen in Figure 4.29 to Figure 4.31. The practical results lie on top of one another and are therefore difficult to distinguish.

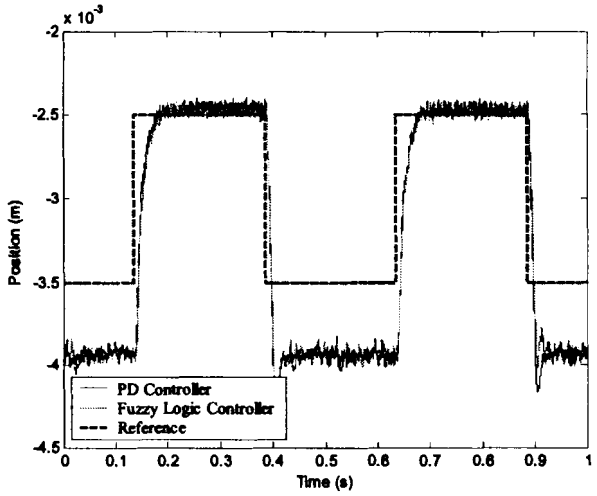

Figure 4.29: Practical comparative results for optimised perturbation (1000 μm)

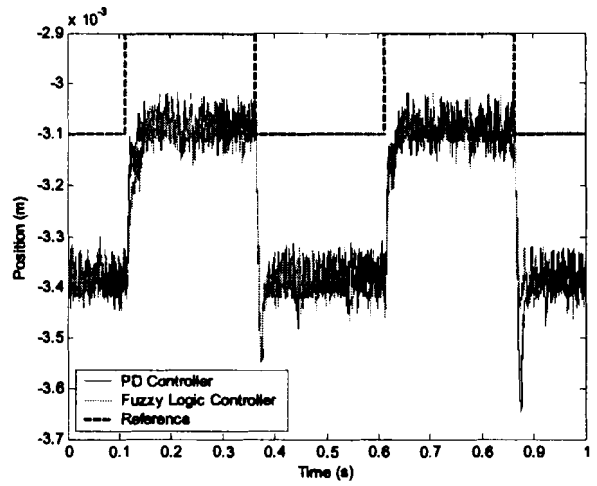

Figure 4.30: Practical comparative results for small perturbation (200 μm)

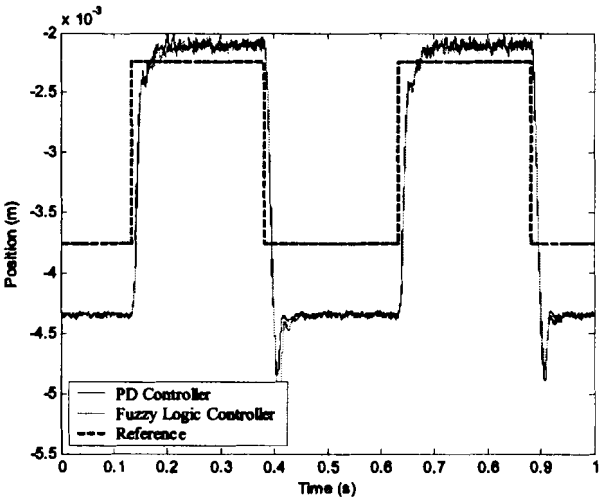

Figure 4.31: Practical comparative results for large perturbation (1500 μm)

4.5 Conclusion

The aim of this chapter was to implement an optimised linear PD controller and to derive an equivalent linear fuzzy logic controller. From the comparative results it is clear that an equivalent linear fuzzy logic controller can be realised to perfectly mimic the response of a PD controller.

By being able to realise fuzzy control in both the simulation of the model and in the practical model to correlate so closely to the optimised PD controller, it is expected that a fuzzy controller is either equivalent or superior to a classical PD controller. By delinearising the fuzzy controller it is inevitable that the fuzzy controller has to be superior.

Chapter 5

Nonlinear Control

5.1 Introduction

In chapter 2 a couple of nonlinear control techniques were discussed. A decision was taken that the sliding mode control technique would be a suitable nonlinear controller to implement on the axial AMB. It was apparent from the studied literature that sliding mode control would be suitable for implementation on the AMB system because this method of control has frequently been applied to AMB systems. The performance of the sliding mode controller will be compared to that of the linear controllers implemented in the previous chapter.

In this chapter a sliding mode control law will be derived for an axial AMB system operated in the differential driving mode. The implementation of this control law on a simulation as well as a practical model will be discussed.

5.2 Sliding mode control

In the formulation of any control problem there will typically be discrepancies between the actual plant and the mathematical model developed for controller design. This mismatch may be due to unmodelled dynamics, variation in system parameters or the approximation of complex plant behaviour by a straightforward model. The engineer must ensure that the resulting controller has the ability to produce the required performance levels in practice despite such plant/model mismatches. This has led to the development of so-called robust control methods which seek to solve this problem. One particular approach to robust control controller design is the so-called sliding mode control methodology [17].

Sliding mode control is a particular type of Variable Structure Control. Variable Structure Control Systems (VSCS) are characterized by a suite of feedback control laws and a decision rule. The decision rule, termed the switching function, has as its input some measure of the present system behaviour and produces as an output the particular feedback controller which should be used at that instant in time. A variable structure system may be regarded as a combination of subsystems where each subsystem has a fixed control structure and is valid for specified operating regions of the system. One of the advantages of introducing this additional

complexity into the system is the ability to combine useful properties of each of the composite structures of the system. Furthermore, the system may be designed to possess new properties not present in any of the composite structures alone.

Variable structure control systems evolved from the pioneering work of Emel'yanov and Barbashin in the early 1960s. The ideas did not appear outside of Russia until the mid 1970s when a book by Itkis (1976) and a paper by Utkin (1977) were published in English. The ideas have successfully been applied to problems as diverse as automatic flight control, control of electric motors, chemical processes, helicopter stability augmentation systems, space systems and robots.

In sliding mode control, the VSCS is designed to drive and then constrain the system state to lie within a neighbourhood of the switching function. There are two main advantages to this approach. Firstly, the dynamic behaviour of the system may be tailored by the particular choice of switching function. Secondly, the closed-loop response becomes totally insensitive to a particular class of uncertainty. The latter invariance property clearly makes the methodology an appropriate candidate for robust control. In addition, the ability to specify performance directly makes sliding mode control attractive from the design perspective [17].

5.2.1 Sliding mode control background

Consider the second order-system in (33):

$$\ddot{x} = f(\mathbf{x}) + u \tag{33}$$

where x is the output, u is the control input and $\mathbf{x} = \left[x \ \dot{x} \ \ldots \ x^{(n-1)} \right]^T$ is the state vector. The function $f(\mathbf{x})$ is not exactly known due to the inaccuracies in the model. The aim is to get the state $\mathbf{x}$ to track a specific time varying state $\mathbf{x}_d = \left[x_d \ \dot{x}_d \ \ldots \ x_d^{(n-1)} \right]^T$ (desired state) in the presence of modelling uncertainties.

Let $\tilde{x} = x - x_d$ be the tracking error in the output variable x, and let

$$\tilde{\mathbf{x}} = \mathbf{x} - \mathbf{x}_d = \left[\tilde{x}\ \dot{\tilde{x}}\ \ldots\ \tilde{x}^{(n-1)}\right]^T \tag{34}$$

be the tracking error vector.

A time varying surface $S(t)$ is also defined in the state space $\mathbf{R}^{(n)}$ by $s(\mathbf{x};t) = 0$, where

$$s(\mathbf{x};t) = \left(\frac{d}{dt} + \lambda\right)^{n-1} \tilde{x} \tag{35}$$

and λ is a positive constant.

For the system in (33)

$$s = \dot{\tilde{x}} = \lambda\tilde{x} \tag{36}$$

The simplified 1st-order problem of keeping the scalar s at zero can be achieved by choosing the control law u in (33) such that outside $S(t)$

$$\frac{1}{2}\frac{d}{dt}s^2 \le -\eta|s| \tag{37}$$

where η is a positive constant.

In effect (37) states that the squared distance to the surface, measured by s^2, decreases along all system trajectories. This implies that all system trajectories point towards the surface $S(t)$ as shown in Figure 5.1.

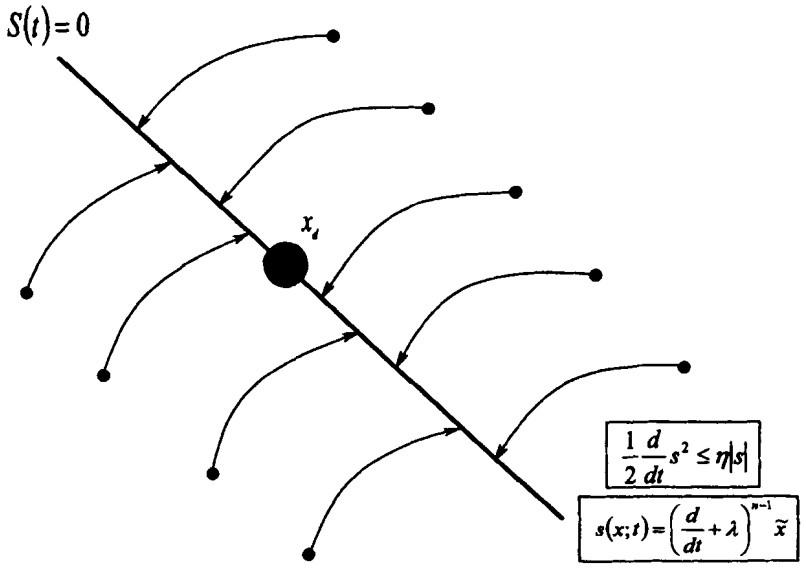

Figure 5.1: Sliding condition

When the system trajectories reach the surface, $S(t)$, they remain on it. If $S(t)$ verifies (37), it is called a sliding surface. The sliding surface is a line in the phase plane with a slope of $-\lambda$ which contains the point x_d.

If the state of the system is not on the surface $S(t)$, by satisfying (37) the surface will still be reached in a finite time t_{reach}, due to the system trajectory as mentioned in the paragraph above. By integrating (37) between t_{state} and t_{reach} it follows that

$$t_{reach} \leq \frac{s(t_{state})}{\eta} \tag{38}$$

When the state has reached the surface after t_{reach}, it then slides towards x_d exponentially with a time-constant of $1/\lambda$ as shown in Figure 5.2. It can be derived that the parameters η and λ influence the time response of the system.

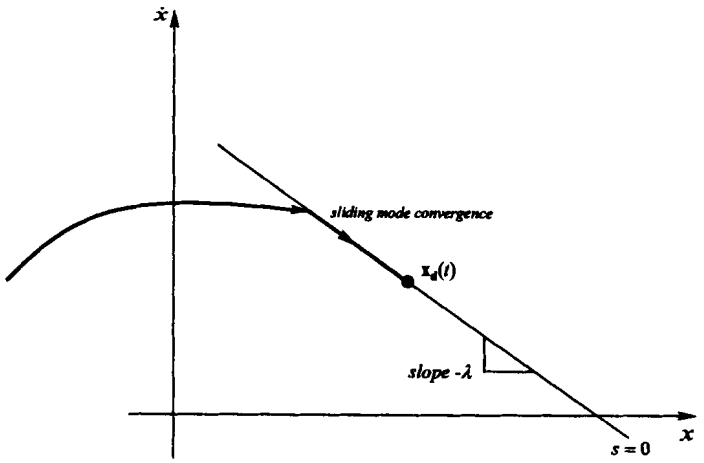

Figure 5.2: Desired state convergence

The idea behind (35) and (37) is to lock on to a well behaved function of the tracking error s, according to (35), and then select the feedback control law u in (33) such that s^2 remains a Lyapunov-like function of the closed loop system in the presence of modelling inaccuracies and disturbances.

The controller design consists of the two following steps.

- Step 1:

  A feedback control law u is selected to satisfy (37). To accommodate modelling imprecision and disturbances, the control law has to be discontinuous across $S(t)$. Due to inevitable imperfect control switching chattering is experienced. Chattering is undesired in practice, with the exception of a few applications, since it involves high control activity and therefore leads to step 2.

- Step 2:

  The discontinuous control law u is suitably smoothed to achieve an optimal trade-off between control bandwidth and tracking precision.

The first step accounts for parametric uncertainty, while the second achieves robustness to high-frequency unmodelled dynamics.

5.2.2 Controller design

5.2.2 (a) Control law selection

The objective of the controller is to maintain the levitation height $x(t)$, of the disk at a desired height, $x_d(t)$. The tracking error is therefore defined as:

$$\tilde{x}(t) = x(t) - x_d(t) \tag{39}$$

Note that $x_d(t)$ is a function of time due to the fact that it may be time varying.

The sliding surface is defined as follows:

$$S(t) = \dot{\tilde{x}}(t) + \lambda\tilde{x}(t) \tag{40}$$

The objective of sliding mode control is to achieve $S(t) = 0$. The attraction condition for $S(t) = 0$ is

$$S(t)\dot{S}(t) < 0 \tag{41}$$

and

$$\dot{S} = -\eta\,\mathrm{sign}(S(t)) \tag{42}$$

Following from (40), (43) is realised:

$$\dot{S}(t) = \ddot{\tilde{x}}(t) + \lambda\dot{\tilde{x}}(t) \tag{43}$$

but it follows from (39) that

$$\ddot{\tilde{x}} = \ddot{x} - \ddot{x}_d \tag{44}$$

Thus

$$\dot{S}(t) = \ddot{x}(t) - \ddot{x}_d + \lambda\dot{x}(t) \tag{45}$$

By substituting (41) into (42), (46) is obtained.

$$\ddot{x}(t) - \ddot{x}_d + \lambda\dot{\tilde{x}}(t) = -\eta sign(S(t)) \tag{46}$$

The model of the system derived in (5) is

$$\ddot{x}(t) = \frac{k}{m}\frac{u_{m1}{}^2}{x_1{}^2} - \frac{k}{m}\frac{u_{m2}{}^2}{|x_2|^2} - g \tag{47}$$

Therefore

$$\frac{k}{m}\frac{u_{m1}^{\ 2}}{x_1^{\ 2}}-\frac{k}{m}\frac{u_{m2}^{\ 2}}{|x_2|^2}-g=\ddot{x}_d-\lambda\dot{\tilde{x}}-\eta sign(S) \tag{48}$$

By doing symmetrical control around a certain bias current as shown in Figure 5.3 (49) and (50) is obtained.

$$u_{m1}^{\ 2}=I_0^{\ 2}+u_1^{\ 2} \tag{49}$$

$$u_{m2}^{\ 2}=I_0^{\ 2}-u_1^{\ 2} \tag{50}$$

Figure 5.3 shows the procedure followed to determine the control signal. The obtained control signal is an approximation. It is approximated to simplify the determination of the control law and to spare computational power of the implemented controller.

Figure 5.3 is a block diagram of the control system. The output of the controller is the squared value of the control signal and therefore this signal has to be added to the square of the bias current and the produced signal rooted to produce the control signal.

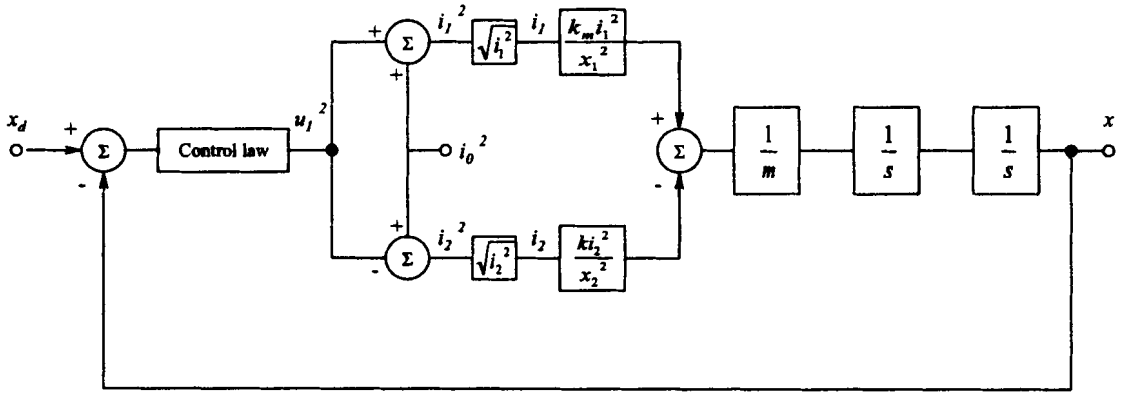

Figure 5.3: : Block diagram of symmetrical control around a bias current i_0

Equation (48) is simplified to realise (51).

$$\frac{u_{m1}^{\ 2}}{x_1^{\ 2}}-\frac{u_{m2}^{\ 2}}{|x_2|^2}=\frac{m}{k}\left[\ddot{x}_d-\lambda\dot{\tilde{x}}-\eta sign(S)+g\right] \tag{51}$$

Equations (49) and (50) are substituted into (51) to get (52). Equation (52) can then be simplified to obtain the control law in (53).

$$\frac{I_0^2+u_1^2}{x_1^2}-\frac{I_0^2-u_1^2}{|x_2|^2}=\frac{m}{k}\left[\ddot{x}_d-\lambda\dot{\tilde{x}}-\eta sign(S)+g\right] \tag{52}$$

$$I_0^2\left[\frac{1}{x_1^2}-\frac{1}{|x_2|^2}\right]+u_1^2\left[\frac{1}{x_1^2}+\frac{1}{|x_2|^2}\right]=\frac{m}{k}\left[\ddot{x}_d-\lambda\dot{\tilde{x}}-\eta sign(S)+g\right]$$

$$u_1^2\left[\frac{1}{x_1^2}+\frac{1}{|x_2|^2}\right]=\frac{m}{k}\left[\ddot{x}_d-\lambda\dot{\tilde{x}}-\eta sign(S)+g\right]-I_0^2\left[\frac{1}{x_1^2}-\frac{1}{|x_2|^2}\right]$$

$$u_1^2=\frac{m\left[\ddot{x}_d-\lambda\dot{\tilde{x}}-\eta sign(S)+g\right]}{k\cdot\left[\frac{1}{x_1^2}+\frac{1}{|x_2|^2}\right]}-\frac{I_0^2\left[\frac{1}{x_1^2}-\frac{1}{|x_2|^2}\right]}{\left[\frac{1}{x_1^2}+\frac{1}{|x_2|^2}\right]} \tag{53}$$

This control law results in chattering due to the discontinuous $\text{sign}(S(t))$ function as shown in Figure 5.4 and the following step is thus smoothing.

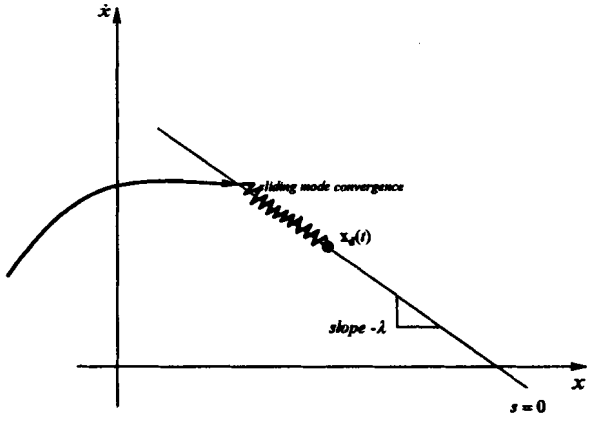

Figure 5.4: Chattering as a result of imperfect control switchings

5.2.2 (b) Smoothing

The problem of chatter can be improved by control smoothing approximations. One of the methods that is applicable is by replacing the infinite gain of $S(t)$ at $S(t)=0$ with a finite gain

when the magnitude of $S(t)$ is smaller than a prescribed value ϕ. This can be done by replacing the $\text{sign}(S(t))$ function with:

$$\text{sat}(S(t)/\phi) := \begin{cases} \text{sign}(S(t)) & \text{if } |S(t)| \geq \phi \\ \dfrac{S(t)}{\phi} & \text{if } |S(t)| < \phi \end{cases} \tag{54}$$

The control law then becomes

$$u_1^2 = \frac{m\left[\ddot{x}_d - \lambda\dot{\tilde{x}} - \eta \cdot sat\left(\frac{S}{\phi}\right) + g\right]}{k \cdot \left[\frac{1}{x_1^2} + \frac{1}{|x_2|^2}\right]} - \frac{I_0^2\left[\frac{1}{x_1^2} - \frac{1}{|x_2|^2}\right]}{\left[\frac{1}{x_1^2} + \frac{1}{|x_2|^2}\right]} \tag{55}$$

This smoothing reduces control activity and also achieves robustness to high frequency unmodelled dynamics.

5.2.3 Results

With the simulated model representing the practical model with remarkable accuracy the derived control law in (55) could be confidently implemented in the simulation. The control variables λ, η and ϕ could be iteratively adjusted to obtain an optimised controller. The values decided on for the variables are $\lambda = 850$, $\eta = 57$ and $\phi = 0.9$.

The stiffness of the AMB system with the sliding mode controller was once again determined by disturbing the suspended disc with a 3 kg upward force and determining the position deviation. The position deviation for the 3 kg disturbance force is shown in Figure 5.5. The stiffness was determined as 140.4 kN/mm in (56).

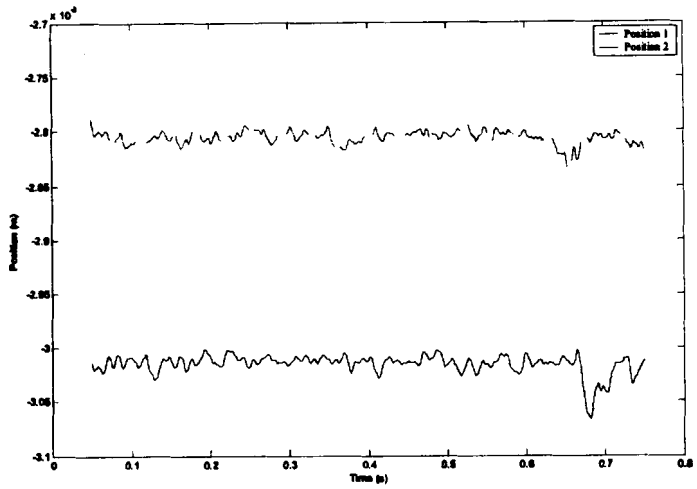

Figure 5.5: Position deviation for determination of stiffness

$$k_{eq} = \frac{f_{disturb}}{\Delta x} = \frac{3 \cdot 9.81}{(-0.00301 - -0.00280)} \quad (56)$$
$$140.4 \text{ kN/mm}$$

The damping of the system was once again determined from the time constant of the step response in (58).

$$-\frac{1}{\tau} = \frac{-b_{eq} + \sqrt{b_{eq}^2 - 4 \cdot m \cdot k_{eq}}}{2 \cdot m} \quad (57)$$

$$-\frac{1}{17.1 \times 10^{-3}} = \frac{-b_{eq} + \sqrt{b_{eq}^2 - 4 \cdot 2 \cdot 140.442 \times 10^3}}{2 \cdot 2} \quad (58)$$
$$b_{eq} = 2518.5 \text{ N.s/mm}$$

The control law derived in (55) was implemented on the simulation model and intuitively optimised for a step response for a 1000 μm step input as shown in Figure 5.6(a). This optimised controller was then implemented on the practical model via dSpace and Simulink®. The step response for a step input of a 1000 μm is shown in Figure 5.6(b).

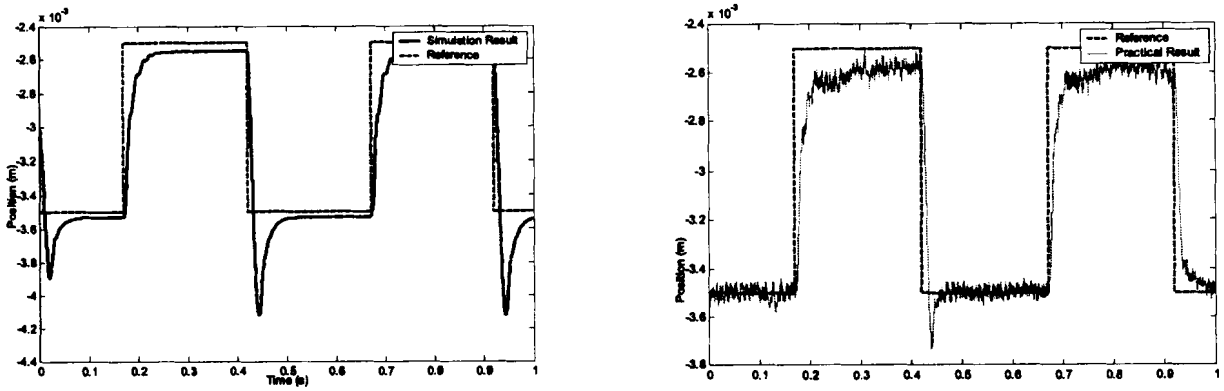

(a) (b)

Figure 5.6: Sliding mode controller results for optimised perturbation (1000μm)

Figure 5.7 shows the correlation between the simulated and practical results to the step response. The dynamic responses of the simulated and practical systems correlate reasonably well. The simulated response displays a large negative overshoot which is not as prominent in the practical result. This inconsistency may be due to the difference in the implementation techniques used for the two systems.

The dSpace technology used to implement the controller on the practical model does not support the Simulink® simulation block "MATLAB Fcn" for the implementation of the control law. The control law had to be constructed by using a series of different Simulink® simulation blocks. The possibility that these blocks do not perfectly match the methods used in the MATLAB simulation is likely.

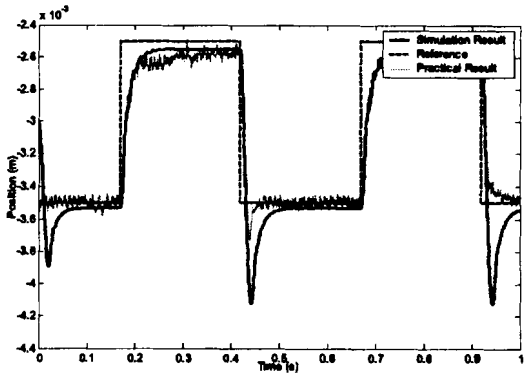

Figure 5.7: Comparative simulation and practical results (1000 μm)

The responses also display a difference in steady state error. This discrepancy is due to the thermal drift of the different components in the system. The most likely component causing this off-set is the sensor.

Figure 5.8 shows the step responses of the simulated and practical models for a 200 μm reference step input.

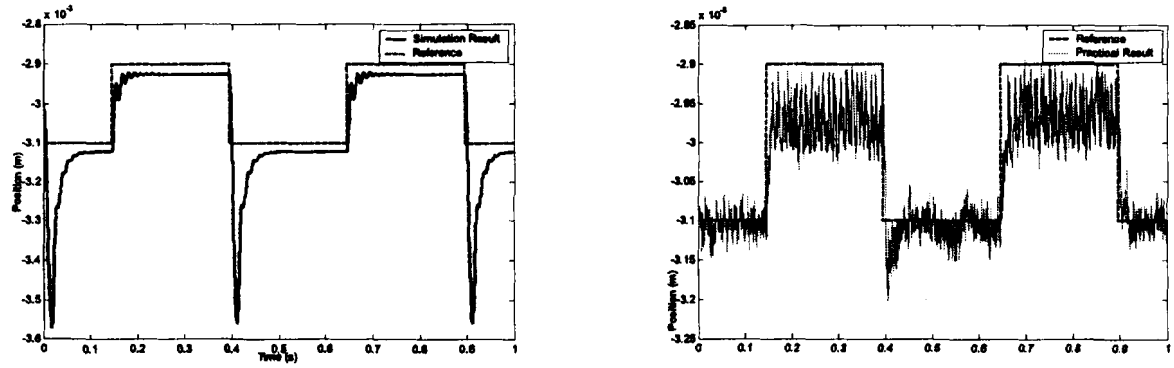

(a) (b)

Figure 5.8: Sliding mode controller results for small perturbation (200 μm)

Figure 5.9 shows the comparison between the practical and simulated step responses of the 200 μm perturbation. The negative overshoot in the simulated result is very prominent in this result.

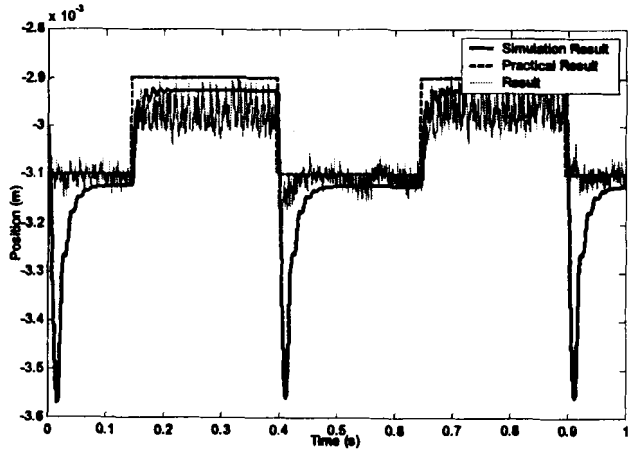

Figure 5.9: Comparative simulation and practical results (200 μm)

Figure 5.10 shows the step responses of the simulated and practical models for a 1500 μm reference step input.

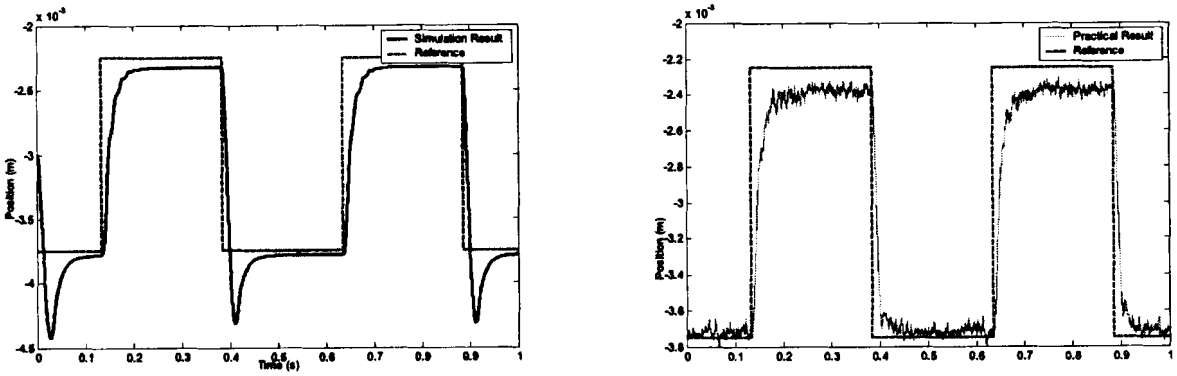

(a) (b)

Figure 5.10: Sliding mode controller results for large perturbation (1500μm)

Figure 5.11 shows the comparison between the practical and simulated results for the two models. Here the negative overshoot is still present in the simulated result, but totally absent in the practical result.

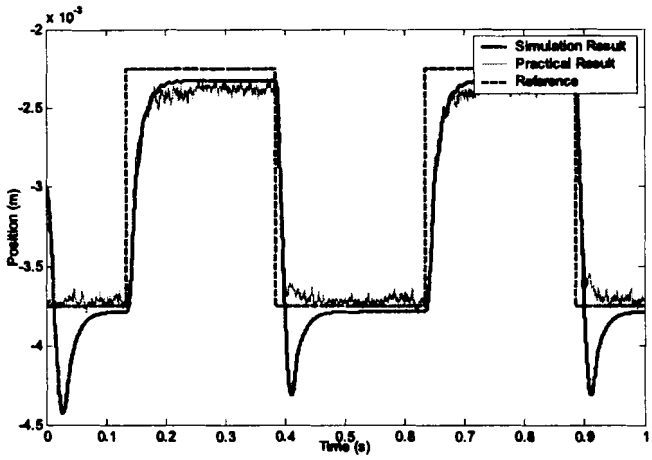

Figure 5.11: Comparative simulation and practical results (1500 μm)

5.3 Conclusion

The goal of this chapter was to derive a sliding control law for an axial AMB system that is operated in the differential driving mode. This was accomplished and the derived controller was implemented on the simulation model

It was found that due to the increased complexity of the sliding mode controller over the linear controller it was not as simple to implement the controller on the practical model. An equivalent Simulink® model had to be constructed with individual Simulink® simulation blocks. This lead to discrepancies between the simulated and practical results.

Chapter 6

Conclusion and recommendations

6.1 Introduction

In this dissertation three different controllers were implemented on an axial AMB system. The purpose of the study was to determine which of the three control methods exhibited the best performance when exposed to disturbances. The controllers were divided into two different categories namely linear controllers and nonlinear controllers. A PD controller and a linear fuzzy logic controller were investigated under the category of linear controllers. Although fuzzy logic controllers are defined as nonlinear controllers, the one used in the investigation was configured to exhibit linear behaviour. A sliding mode controller was investigated as the nonlinear controller.

6.2 Comparative discussion

The criteria used to compare the controllers were the equivalent stiffness, equivalent damping and the ITAE of the three controllers. The ITAE was chosen as a suitable performance index because it reduces the contribution of the large initial error to the value of the performance integral, as well as to emphasise errors occurring later in the response [4]. The ITAE performance indices were determined by calculating an ITAE index for a positive and negative step of 1000 μm respectively. The two indices were then added to determine the comparative index. This method was followed to ensure that no discrimination occurred against a controller when the performance differed between the positive and the negative step response of the implemented controllers. The values for the different criteria were determined for both the simulated and the practical results and Table 6.1 shows the comparison between the different controllers and the comparison between the simulated and practical results.

For all the controllers the simulated and practical results display remarkably close correlation. This indicates that the simulation model closely emulates reality. The only result where a discrepancy is visible between the simulated and practical results is the ITAE index for the sliding mode controller. This inconsistency is due to the large negative overshoot displayed in the simulated results which is not present in the practical results.

Table 6.1: Controller comparisons

Performance comparison of the implemented controllers				
		PD controller	**Fuzzy logic controller**	**Sliding mode controller**
Equivalent stiffness	***Practical***	79.8 kN/m m	88.6 kN/m m	140.4 kN/mm
	Simulated	70.5 kN/mm	97.6 kN/mm	110.8 kN/mm
Equivalent damping	***Practical***	1246.1 N.s/mm	1558.6 N.s/mm	2031.2 N.s/mm
	Simulated	1351.5 N.s/mm	1351.5 N.s/mm	2011.8 N.s/mm
ITAE	***Practical***	3.0713×10^{-5}	2.7382×10^{-5}	7.5977×10^{-6}
	Simulated	2.3573×10^{-5}	1.9741×10^{-5}	1.5140×10^{-5}

The results of the PD and fuzzy logic controllers correlate remarkably well due to the fact that the two controllers were configured to be equivalent. Considering that the AMB is a highly nonlinear system it is expected that the fuzzy controller which is defined as a nonlinear controller should be able to provide a totally superior performance after it is delinearised.

When comparing the linear controllers to the nonlinear sliding mode controller it is visible that the performance of the nonlinear controller is superior to those of the linear ones in all aspects. For large perturbations around the operating point the sliding mode controller has total superiority over the linear controllers. This is because the linear controllers cannot compensate for large deviations from the linearised operating point of the model where the nonlinear controller can accommodate modelling imprecision.

6.3 Conclusions

During the study it was found that the system on which the study was performed was not totally suitable and some changes were made to improve the suitability of the system for a comparative study.

The first improvement made was to replace the voltage controlled power amplifier with a linear current controlled amplifier. This change was a vast improvement but still was not ideal. Problems encountered with the new amplifier included complicated simulation and poor slew rate. The latter problem was induced into the system as a result of an electromagnet which was

not ideal with a very high inductance and resistance. This resulted in a reduced bandwidth of the system.

The sensor of the system also did not match the application. When using an inductive sensor for an application with a large airgap the sensor becomes highly nonlinear. This problem was addressed by using different linearisation techniques. Another problem encountered with the sensor was its susceptibility to noise and thermal drift. These factors made repeatability of the system very difficult which is undesirable for a comparative study.

6.4 Recommendations

The results achieved during the study were good enough to objectively compare the linear and nonlinear controllers studied. Improved results may however be achieved by doing the following:

The fuzzy logic controller was configured to emulate the linear PD controller. By achieving this goal, the deduction was made that a fuzzy logic controller performs just as well as a PD controller or better. This statement can be verified by delinearising the membership functions to explore the full potential of the controller.

During the implementation of the sliding mode controller it was found that the dynamic behaviour of the MATLAB® m-code simulation and the practical results did not correlate as well as predicted. This discrepancy was attributed to the difference between execution of the m-code simulation and that of Simulink® used to implement the controller via dSPACE. This difference can be investigated to achieve closure on the matter.

The technical detail of sliding mode control did not become completely clear during the course of the study. A specialised study can be done to completely understand this method of control and to fully utilise its potential.

The inductive sensor used on the model was found to be inappropriate for the specific study. By improving the sensor improved control performance can be achieved by all the controllers and a better comparison can be made between them.

6.5 Closure

The goals of the study were achieved by implementing three different control techniques on an axial AMB and sensibly comparing them to one another. The foundation is laid for specialised investigation on modern control techniques.

Appendix A

A.1 Data CD

- MATLAB® Code
- Simulink® implementation models
- dSPACE experiment files
- Dissertation in MS Word format

A.2 Simulink® models

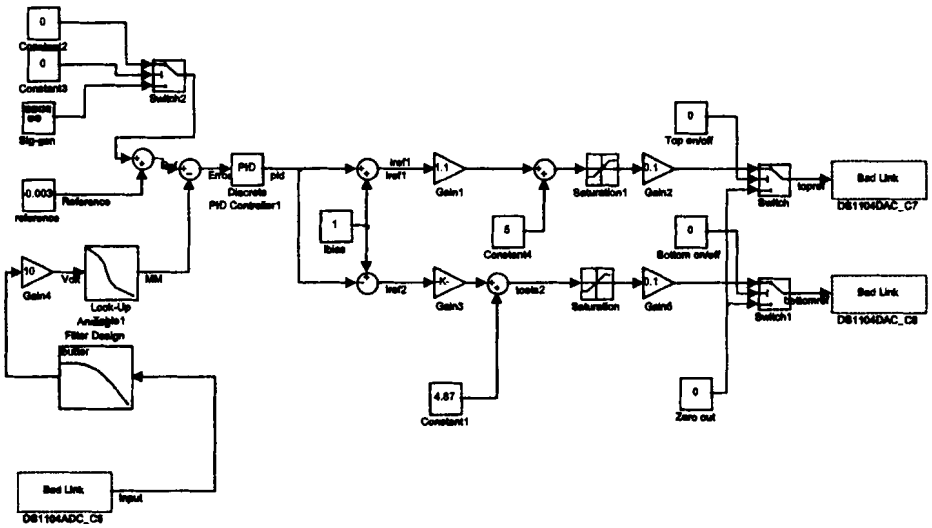

Figure A.1: Simulink® model for PD control

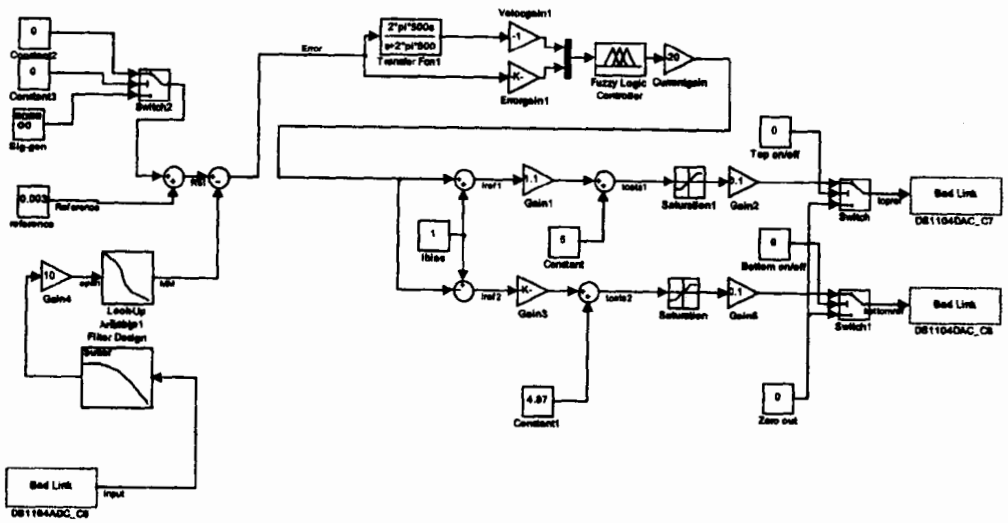

Figure A.2: Simulink® model for equivalent linear fuzzy control

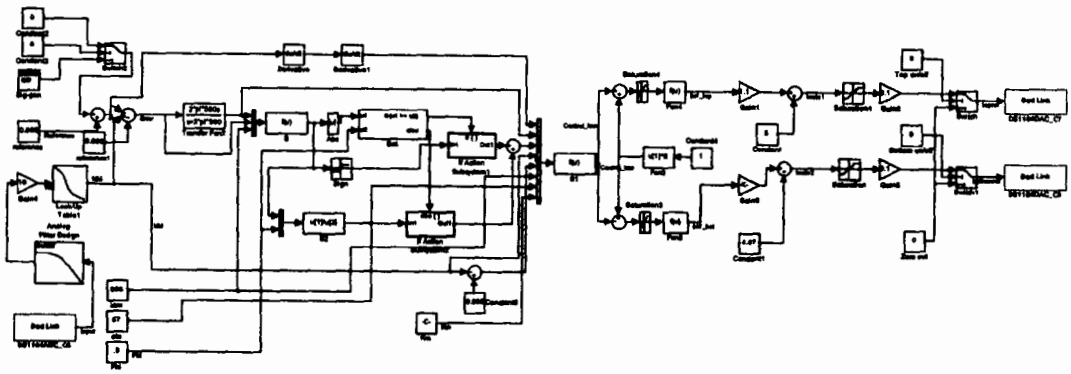

Figure A.3: Simulink® model for sliding mode control

A.3 Photos

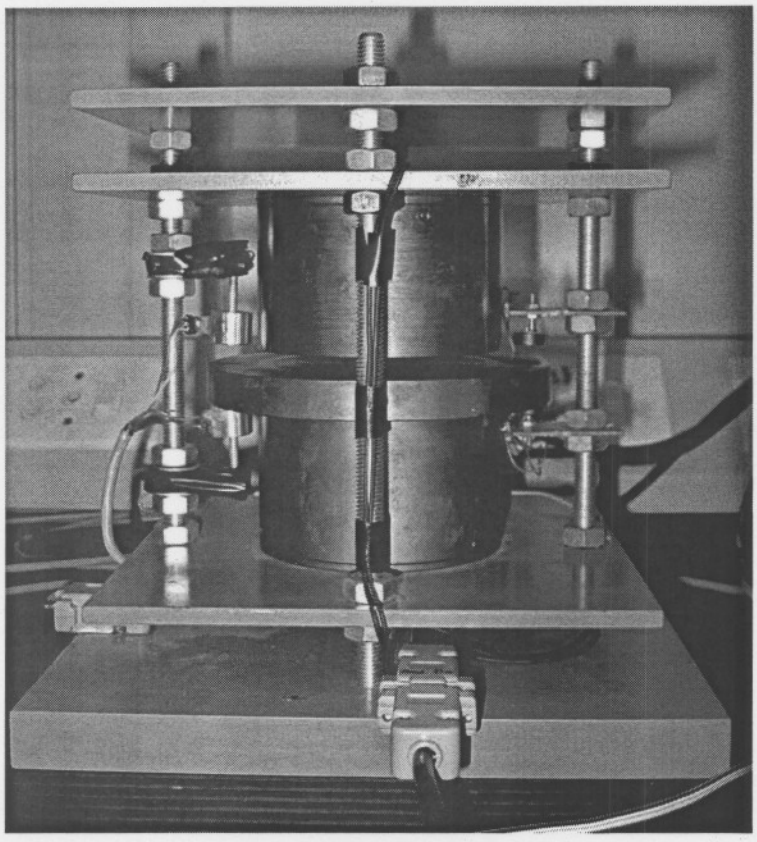

Figure A.4: Electromagnet configuration

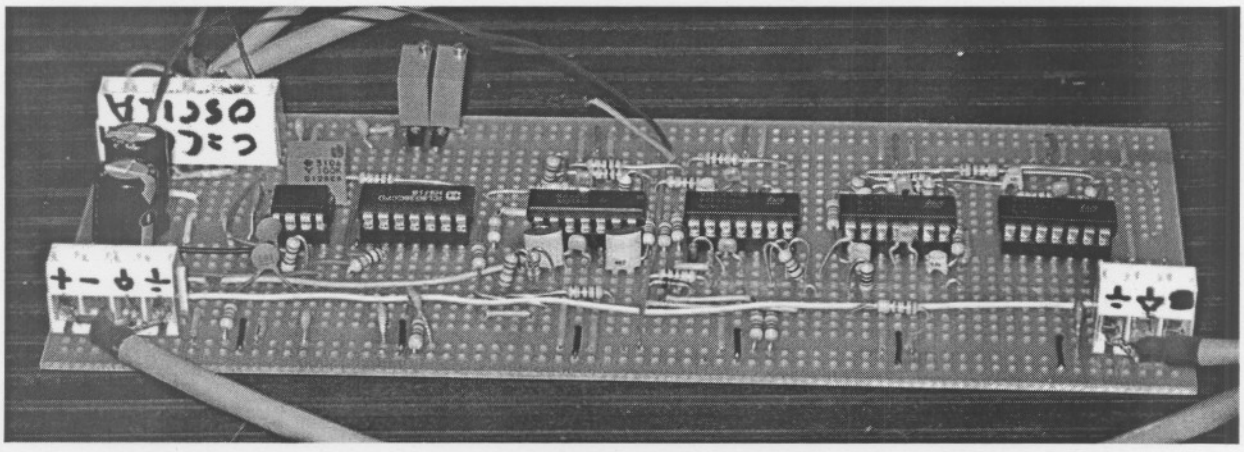

Figure A.5: Inductive sensor circuit

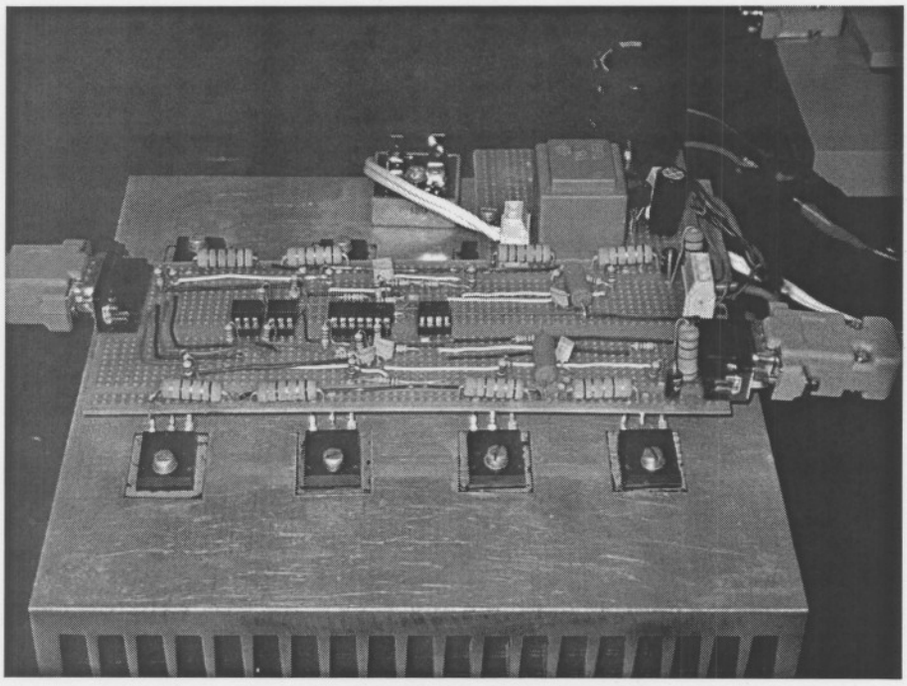

Figure A.6: Linear power amplifier

References

[1] IST Ltd. PBMR. Available: http://www.istltd.com/nuclear/pbmr.asp [Date of access: November 2005].

[2] J.D. Nel, "The development of a radial active magnetic bearing," Dissertation M.Eng, North-West University, Potchefstroom Campus, 2004

[3] M.E.F. Kaskarda and P.E. Allaire. (1997, Jan). The measurement and characterization of power losses in high speed magnetic bearings. ROMAC Report No. 407.

[4] R.D. Dorf and R.H. Bishop, "Modern control systems," Prentice-Hall, 2001

[5] E.O. Ranft, "The Development of a Flexible Rotor Active Magnetic Bearing System," Dissertation M.Ing, North-West University, Potchefstroom, 2004

[6] J.-J.E. Slotine and W. Li, "Applied Nonlinear Control," Prentice-Hall, 1991.

[7] R. Sepulchre, M. Jankovic and P. Kokotovic "Constructive Nonlinear Control," Springer-Verlag, London, 1997

[8] K.J. Åström and B. Wittenmark, "Adaptive control," Addison Wesley, 1995

[9] D.E. Kirk, "Optimal control theory an introduction," Prentice-Hall, 1970

[10] R. Gouws, "The development of an axial active magnetic bearing," Dissertation M.Ing, North-West University, Potchefstroom, 2004

[11] G. Schweitzer, H. Bleuler and A, Traxler, "Active Magnetic Bearings," Zürich :Authors working group, 2003

[12] S. Maram, "Hierarchical Fuzzy Controlof the UPFC and SVC located in AEP's Inez Area," Dissertation M.Ing, Virginia Polytechnic Institute and State University, 2003

[13] G. Bojadziev and M. Bojadziev, "Fuzzy sets, fuzzy logic, applications," World Scientific Publishing Co. Pte. Ltd., 1995

[14] Li-Xing Wang, "Adaptive fuzzy systems and control," Prentice Hall, 1994

[15] Matlab® Version 6.5 Release 12, "Fuzzy logic Toolbox 2.1.2 Release notes"

[16] V. Georgescu, "Fuzzy Control Applied to Economic Stabilization Policies," Faculty of Economic Sciences, University of Craiovo, Romania. Available: http:\\www.ici.ro/ici/revista/sic2001/art5.htm [Date of access: June 2005]

[17] C. Edwards and K. Spurgeon, "Sliding mode control – Theory and applications," Taylor & Francis Ltd, 1998

[18] A.P. George, "Introduction to the Pebble Bed Modular reactor (PBMR)," PBMR, Pretoria, Tech. Rep. 2001.

[19] M.C. Nieuwoudt and W Kriel, "PBMR operability summary," PBMR, Pretoria, Tech. Rep. Revision: 2D, 2001.

[20] Revolve Magnetic Bearings Inc. Magnetic bearings. [Online]. Available: http://www.revolve.com/ Technology/magbearings.html, [Date of access: February. 2003].

[21] D.P. Atherton, "Nonlinear control engineering," Van Nostrand Reinhold Company, 1975.

[22] P. Allaire, C.R. Knospe, *et al.* "Short course on magnetic bearings," University of Virginia, United States of America, 1997.

[23] H. Ying, W. Siler, J.J. Buckley, "Fuzzy Control Theory: A Nonlinear Case," *Automatica,* Vol. 26, No 3, pp. 513-520, 1990

[24] J. Jantzen, "Tuning of Fuzzy PID Controllers"

[25] D.Cho, Y. Kato and D. Spillman, "Experimental Comparison of Classical and Sliding Mode Controllers in Magnetic Levitation Systems," *IEEE Control Systems Magazine*, vol 13, pp. 42-48, 1993